




**Measurement of the low-frequency charge noise of bacteria**Yichao Yang , Hagen Gress , and Kamil L. Ekinici \**Department of Mechanical Engineering, Division of Materials Science and Engineering, and the Photonics Center, Boston University, Boston, Massachusetts 02215, USA*

(Received 21 November 2021; accepted 8 June 2022; published 29 June 2022)

Bacteria meticulously regulate their intracellular ion concentrations and create ionic concentration gradients across the bacterial membrane. These ionic concentration gradients provide free energy for many cellular processes and are maintained by transmembrane transport. Given the physical dimensions of a bacterium and the stochasticity in transmembrane transport, intracellular ion concentrations and hence the charge state of a bacterium are bound to fluctuate. Here we investigate the charge noise of hundreds of nonmotile bacteria by combining electrical measurement techniques from condensed matter physics with microfluidics. In our experiments, bacteria in a microchannel generate charge density fluctuations in the embedding electrolyte due to random influx and efflux of ions. Detected as electrical resistance noise, these charge density fluctuations display a power spectral density proportional to  $1/f^2$  for frequencies  $0.05 \text{ Hz} \leq f \leq 1 \text{ Hz}$ . Fits to a simple noise model suggest that the steady-state charge of a bacterium fluctuates by  $\pm 1.30 \times 10^6 e$  ( $e \approx 1.60 \times 10^{-19} \text{ C}$ ), indicating that bacterial ion homeostasis is highly dynamic and dominated by strong charge noise. The rms charge noise can then be used to estimate the fluctuations in the membrane potential; however, the estimates are unreliable due to our limited understanding of the intracellular concentration gradients.

DOI: [10.1103/PhysRevE.105.064413](https://doi.org/10.1103/PhysRevE.105.064413)**I. INTRODUCTION**

Bacteria create and maintain transmembrane concentration gradients of small metal ions, such as potassium and sodium [1,2]. These ionic concentration gradients are the main source of the electrical and electrochemical potentials that are present across the cell membrane and facilitate a number of crucial cellular processes [3–9]. The processes for separation, concentration, and regulation of the inorganic ions by bacteria are made possible by the plasma membrane and the transmembrane proteins embedded in the membrane, as shown in Fig. 1(a). The plasma membrane is a thin but strongly insulating lipid structure, allowing a bacterium to maintain its charge state effectively. The many different transmembrane proteins that are in the bacterial membrane act as channels and pumps for ions [10]. Figure 1(a) also shows the electrical circuit model [5,8,11] of a membrane patch. Here the ion channels and pumps for each ion are modeled as a nonlinear resistor with a conductance that depends on the electrical potential of the membrane,  $V_{\text{mem}}$ , and the Nernst potential,  $E_X$ , for the ion X.

A small and insulating system, such as a bacterium, will be particularly susceptible to charge fluctuations [12–14]. Thus, charge noise should play an important role in bacterial ion homeostasis. Based on the circuit model [Fig. 1(a)], the charge fluctuations within the cytoplasm are the result of two coupled noisy processes. First, the ionic current through the ion channels is noisy [15], with the ensuing fluctuations in intracellular ion concentrations causing voltage noise in  $V_{\text{mem}}$ . Second, any noise originating in  $V_{\text{mem}}$ , e.g., due to a random depolarization

of a membrane patch or even thermal noise [16,17], will cause fluctuations in the transmembrane current [18] and hence the intracellular ion concentrations. Furthermore, these two noise processes will tend to enhance each other. We argue that an equivalent noise voltage,  $e_n$ , should be imposed on  $V_{\text{mem}}$  in Fig. 1(a) in order to account for all the electrical fluctuations present.

Our understanding of how a bacterium regulates the concentrations of metal ions in its cytoplasm (i.e., the intracellular metallome) is far from complete. It is generally assumed that the time-averaged intracellular ion concentrations in a bacterium remain roughly constant [19,20]—indicating charge conservation. Average bacterial ion efflux [21] and influx [22] rates have been determined from concentration measurements in media in which large populations of bacteria are grown. On the other hand, patch clamp measurements on single bacterial ion channels have shown that ion transport is noisy, with the current noise power spectral density (PSD) proportional to  $1/f$  at low frequencies [23]. While the time-averaged charge state remains constant, bacteria surprisingly modulate their membrane potential on the timescale of seconds—as shown in recent fluorescent microscopy experiments [14]. Single cells get hyperpolarized and depolarized spontaneously and repeatedly over time. It has been suggested that these charge fluctuations are purposeful, but little is known about their downstream effects. Thus, bacterial ion homeostasis is expected to be highly dynamic [1] and dominated by strong charge noise. At the present time, quantitative measurements of electrical fluctuations and noise models of single bacterial cells are missing from the biophysics literature, partly due to a lack of sensitive tools on the size scale of a bacterium [14].

\*ekinici@bu.edu

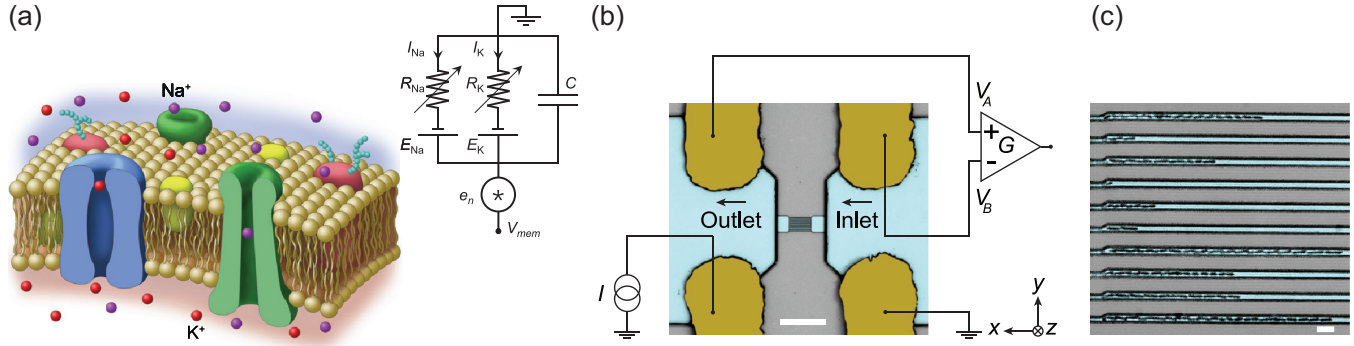


FIG. 1. (a) Illustration of a membrane patch and its circuit model. (b) Microfluidic resistor and the simplified circuit diagram for monitoring its electrical fluctuations. The microchannels in the center of the resistor are filled with nonmotile bacteria. The false-colored inverted microscope image shows the electrodes (gold) and the broth medium (light blue) looking from the bottom glass side of the device. The scale bar is  $200 \mu\text{m}$ . Arrows indicate the direction of the flow. The current source pushes a bias current through the device. The ensuing voltage drop,  $V_A - V_B$ , is detected by a differential amplifier with gain  $G$ . [See Fig. 2(a) below for more details.] (c) Close-up image of the microchannels filled with *K. pneumoniae* cells. Each microchannel has linear dimensions of  $l \times w \times h \approx 100 \times 2 \times 2 \mu\text{m}^3$ ; the cross section reduces to  $800 \text{ nm} \times 2 \mu\text{m}$  at the constriction. The scale bar is  $5 \mu\text{m}$ .

To probe the noisy charge dynamics in bacteria with sufficient time resolution and electrical sensitivity, we have combined low-frequency noise analyses from condensed matter physics [24] with microfluidics [25]. Our overarching hypothesis is that the metabolic activity of bacteria modulates the concentrations of various ions in the medium, leading to detectable fluctuations in the electrical impedance. In Sec. II we present our experimental approach with particular attention to the electrical measurements. The results in Sec. III establish that electrical fluctuations detected from bacteria scale as  $1/f^2$ , with the characteristics of equilibrium resistance noise [26–30]. In Sec. IV we look at possible noise mechanisms and discuss the possibility of charge noise. Section V is reserved for conclusions. In Appendix A we present further experimental details. In Appendix C we discuss how to consistently remove the superficial effects of the measurement circuit from the noise. In Appendix D we present results from our control experiments and discuss perturbations; we also discuss the contribution of another phenomenon, namely the nanomechanical fluctuations of a bacterium, to the observed noise. In Appendix E we present the details of how we estimate various electrical noise quantities.

## II. EXPERIMENTAL APPROACH

### A. Device and setup

#### 1. Microfluidic resistor

We perform our electrical noise measurements in a PDMS microfluidic resistor that sits on an inverted microscope stage. As shown in Fig. 1(b), the device has ten parallel microchannels at its center, each with a nanoscale constriction toward the outlet end [Fig. 1(c)]. The microfluidic resistor is filled with a liquid electrolyte, such as Luria-Bertani (LB) broth medium or phosphate-buffered saline (PBS), and four thin film Cr-Au electrodes allow for electrical contact to the ions in the medium [Fig. 1(b)]. Cr-Au electrodes are a good alternative to AgCl electrodes: they are easy to fabricate and provide satisfactory electrical properties [31–33]. Unless otherwise

noted, the temperature of the media is kept at  $37^\circ\text{C}$  by the temperature-controlled inverted microscope stage.

### 2. Loading and trapping the bacteria

The noise measurements are performed on both live and dead bacteria trapped in these parallel microchannels. At the start of each experiment, we load and trap the bacteria using a pressure-driven flow of a bacteria solution from the inlet toward the nanoconstriction with  $\Delta p \approx 10 \text{ kPa}$ . The bacteria accumulate in the microchannels in a linear fashion, as shown in Fig. 1(c). Once the bacteria are loaded, we wait for 30 min before starting the electrical measurements. During the measurements, we maintain a constant  $\Delta p \approx 0.6 \text{ kPa}$  to ensure the flow of nutrients to the bacteria in the microchannel region, except in experiments for studying the effects of different  $\Delta p$  values. The pressure-driven flow jams the bacteria towards the nanoconstriction and keeps the bacteria from moving; it also prevents the bacteria from oscillating due to the electrokinetic forces.

### 3. Properties of the bacteria

We use nonmotile Gram-negative bacteria (*Klebsiella pneumoniae*) and Gram-positive bacteria (*Staphylococcus saprophyticus*) in our experiments. *K. pneumoniae* is a rod-shaped microorganism that has a length of  $2\text{--}3 \mu\text{m}$  and a cross-sectional area of  $0.8 \mu\text{m}^2$  [34]; *S. saprophyticus* is a spherical microorganism that has a diameter of  $1 \mu\text{m}$  [35]. The average doubling times for *K. pneumoniae* and *S. saprophyticus* in our microfluidic devices at  $37^\circ\text{C}$  are 55 min and 100 min, respectively [25]. In experiments with dead bacteria, the cells are first killed by adding a small amount of glutaraldehyde into the broth medium, before they are pushed into the microchannels. Glutaraldehyde is a fixative which kills bacteria by impeding essential cellular functions but preserves the cellular morphology and ultrastructure for the period of our experiments ( $\sim 3 \text{ h}$ ) [36].

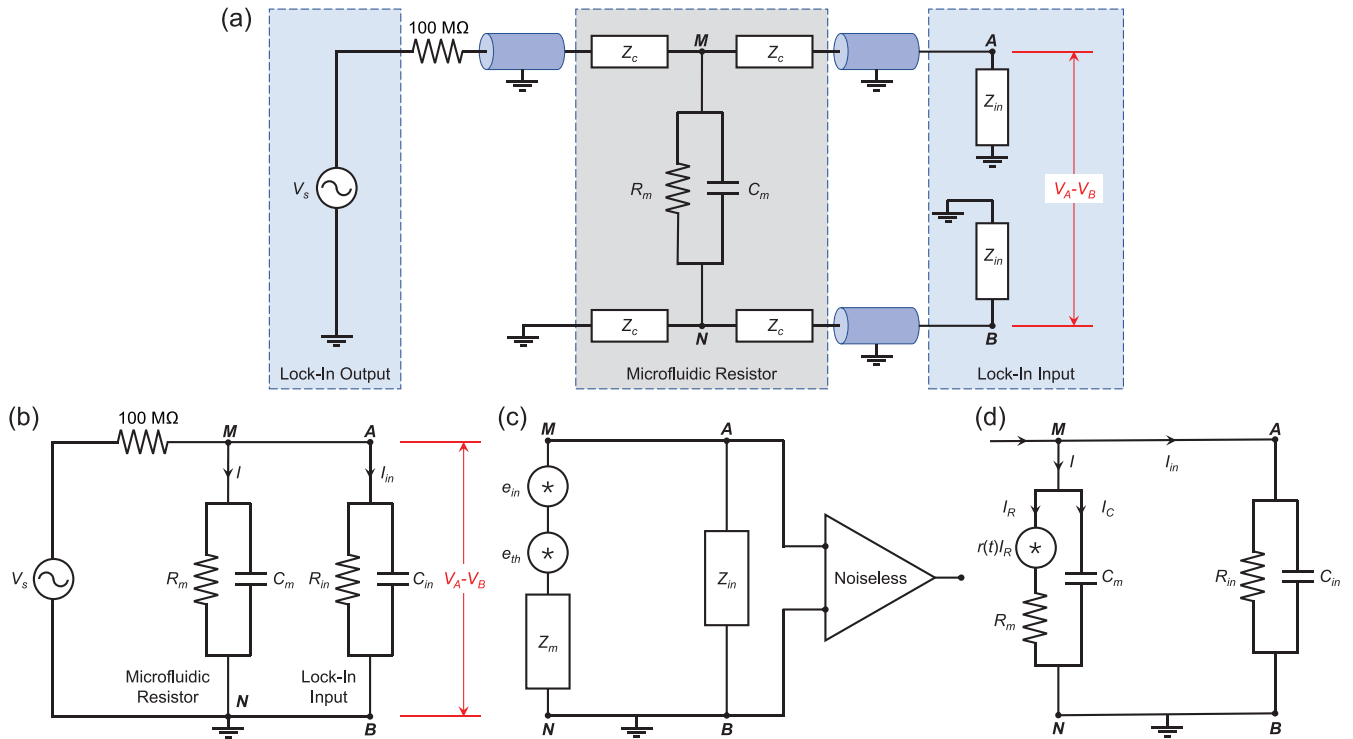


FIG. 2. (a) A schematic diagram of the circuit for electrical measurements. The dashed boxes show the lock-in amplifier reference oscillator output (left), the microfluidic resistor (center), and the lock-in amplifier input (right). (b) A simplified equivalent circuit for the measurement, showing the impedances of the microfluidic resistor and the lock-in input. The arrows show the current flow directions. (c) Thévenin equivalent noise circuit showing the thermal noise of the microfluidic resistor and the input noise of the lock-in amplifier. (d) Equivalent circuit showing the excess noise in the microfluidic resistor.

**B. Electrical measurements**

**1. Lock-in amplifier setup**

We employ a four-probe ac measurement using a lock-in amplifier, as shown schematically in Fig. 1(b) and Fig. 2(a). In Fig. 2(a),  $V_s$  is the reference oscillator output of the lock-in amplifier, with the reference frequency set to  $f_o = 160\text{ Hz}$ ;  $Z_c$  is the contact impedance at each of the four probes; the impedance  $Z_m$  of the microfluidic resistor is modeled as a resistor  $R_m$  in parallel with a capacitance  $C_m$ ; and  $Z_{in}$  is the equivalent impedance of the lock-in amplifier input, with  $V_A - V_B$  representing the voltage drop between the two differential inputs A and B. A current source is created by connecting the lock-in oscillator output in series with a  $100\text{ M}\Omega$  metal film resistor that has a parasitic capacitance  $\leq 0.4\text{ pF}$ . The voltage drop across the microfluidic resistor is measured by the differential voltage detection mode of the lock-in amplifier [Fig. 1(b)].

During the noise measurements, an ac bias current of rms amplitude in the range  $0.70\text{ nA} \leq I \leq 16.50\text{ nA}$  is pushed through the microfluidic resistor, and the voltage fluctuations across the resistor are detected. The time constant and filter roll-off of the lock-in amplifier are 3 ms and 18 dB/oct, respectively, resulting in an equivalent noise bandwidth of 31.25 Hz. The data are transferred to a computer using a digitizer at a sampling rate of 128 Hz. Our subsequent numerical filtering only keeps the noise in the frequency interval  $0.05\text{ Hz} \leq f \leq 10\text{ Hz}$ . To summarize, our measurements are similar to the ac noise measurements on solid state systems

but without the bridge configuration [37]. One big advantage in our system is that we can establish a background noise level by measurements on fixed (dead) bacteria that lack any metabolic activity.

**2. Mean voltage drop and estimation of the circuit parameters**

Figure 3(a) shows the rms value of the mean voltage drop,  $V_{AB} = V_A - V_B$ , for two devices as a function of the rms bias current  $I$  that flows through the devices; the value of the phase angle is  $-34 \pm 3^\circ$  and stays constant. The devices are nominally identical, but one is filled with live cells and the other with dead cells. To find  $I$ ,  $R_m$ , and  $C_m$  [Figs. 2(a) and 2(b)], we first determine the impedances of the  $100\text{ M}\Omega$  resistor, the contact pads, and the lock-in inputs at  $f_o = 160\text{ Hz}$ . We ignore the imaginary component of the  $100\text{ M}\Omega$  resistor. The input impedance  $Z_{in}$  of the lock-in amplifier can be modeled [38] as a resistor,  $R_{in} = 10\text{ M}\Omega$ , in parallel with a capacitor,  $C_{in} = 25\text{ pF}$ , as shown in Fig. 2(b). This gives an equivalent impedance of  $Z_{in} \approx 9.40 - j2.36\text{ M}\Omega$  at  $f_o = 160\text{ Hz}$ . By comparing the results of two-probe measurements to four-probe measurements, we estimate each contact impedance to be  $Z_c \approx 60 - j60\text{ k}\Omega$  and thus negligible. We then calculate  $I$  from the rms lock-in reference voltage value  $V_s$  using Ohm's Law in the simplified circuit shown in Fig. 2(b). Here  $I$  and  $I_{in}$  are the currents that flow through the microfluidic resistor and the amplifier input circuit, respectively. Using these properly determined current values, we then find the values of  $R_m$  and  $C_m$  by linear fitting, i.e., Ohm's Law, as shown

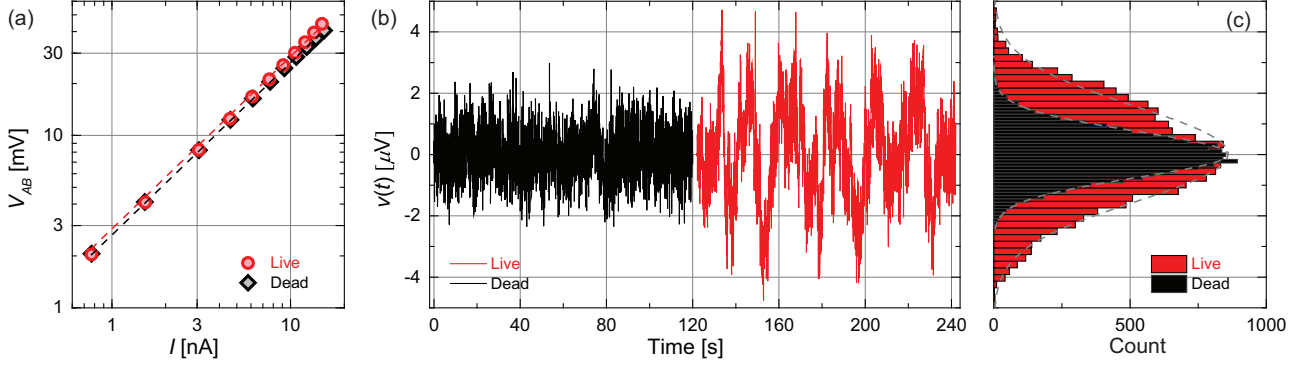


FIG. 3. (a) The  $I$ - $V$  characteristics of devices filled with live and fixed (dead) *K. pneumoniae* cells. The average value of the phase angle is  $-34 \pm 3^\circ$ . (b) Voltage fluctuations  $v(t)$  from live and dead bacteria at a fixed  $I \approx 7.74$  nA bias in a (noise) bandwidth of  $\Delta f \approx 10$  Hz as a function of time. There are  $N \approx 300$  bacteria trapped in both devices. (c) Histograms. The dashed lines show Gaussians.

in Fig. 3(a). These fits yield  $R_m \approx 3.3$  M $\Omega$  and 3.2 M $\Omega$  for live and dead cells, respectively, and  $C_m \approx 0.2$  nF, resulting in  $Z_m \approx 2.30 - j1.50$  M $\Omega$  for both cases. This capacitance value is consistent with the parasitic capacitance of the wiring and the cables. We emphasize that the value of  $R_m$  depends on the number  $N$  of cells trapped in the device [25], and  $N \approx 300 \pm 50$  for both measurements in Fig. 3(a). The  $N$  value, however, will be varied in some measurements, and its effects will be deconvoluted from the measurements, as described below.

### 3. Johnson-Nyquist noise

Now, we turn to a typical noise data trace and discuss the general features of noise. Figure 3(b) shows the time-domain voltage fluctuations,  $v(t)$ , measured across the microfluidic resistor filled with roughly 300 cells in LB for a bias current of  $I \approx 7.74$  nA in a (noise) bandwidth of  $\Delta f \approx 10$  Hz. Within the 120 s data trace, the bacteria do not divide or move into and out of the microchannels. The rms value of the voltage noise can be found as  $1.55$   $\mu$ V for live cells (red) and  $0.76$   $\mu$ V for fixed cells (black). The probability distribution of the noise in both cases is nearly Gaussian [Fig. 3(c)].

To understand the origin of this noise, we first estimate the Johnson-Nyquist noise of the microfluidic resistor and the input noise of the lock-in amplifier, which together should result in a white thermal spectrum away from the carrier. The diagram of the Thévenin equivalent noise circuit is shown in Fig. 2(c). Here  $Z_m$  is the source impedance,  $Z_{in}$  is the amplifier input impedance, and  $e_{th}$  is the thermal noise voltage generated by the source impedance with a PSD of  $4k_B T \text{Re}\{Z_m\}$  with  $\text{Re}$  denoting the real part of the complex impedance. We approximate the noise arising from the amplifier as follows. We assume that the amplifier adds the equivalent input-referred voltage noise  $e_{in}$  to the thermal noise, as shown in Fig. 2(c). We note that the current noise of the amplifier is also lumped into  $e_{in}$ . Then the measured voltage noise PSD with respect to the reference nodes A and B in Fig. 2(c) becomes

$$\begin{aligned} S_V^{(th)}(f, 0) &= \left[ 4k_B T \text{Re}\{Z_m\} + \frac{\langle e_{in}^2 \rangle}{\Delta f} \right] \frac{|Z_{in}|^2}{|Z_m + Z_{in}|^2}, \\ &= 4k_B T R_n. \end{aligned} \quad (1)$$

Here  $S_V^{(th)}(f, 0)$  indicates that the bias current is zero and  $\Delta f$  is the measurement bandwidth. The resistance  $R_n$  is an equivalent noise resistance representing all the white thermal noise sources in the system. To determine  $\langle e_{in}^2 \rangle / \Delta f$  of the lock-in amplifier for our sensitivity setting and source impedance value at 160 Hz, we measure the output noise in separate experiments as a function of source resistance [39]. These measurements allow us to find the equivalent input-referred voltage noise PSD and the equivalent input-referred current noise PSD for each amplifier input as approximately  $1.70 \times 10^{-15}$  V<sup>2</sup>/Hz and  $2.30 \times 10^{-27}$  A<sup>2</sup>/Hz, respectively. Since the lock-in amplifier is used in the  $V_A - V_B$  mode in our measurements, we calculate the total input-referred noise PSD from the amplifier inputs by adding the noise PSDs from each amplifier input, leading to  $\langle e_{in}^2 \rangle / \Delta f \approx 3.85 \times 10^{-14}$  V<sup>2</sup>/Hz. Finally, by substituting  $Z_m \approx 2.30 - j1.50$  M $\Omega$  (for 300 cells),  $Z_{in} \approx 9.40 - j2.36$  M $\Omega$ , and  $\langle e_{in}^2 \rangle / \Delta f \approx 3.85 \times 10^{-14}$  V<sup>2</sup>/Hz into Eq. (1), we find the white noise PSD at the output to be approximately  $S_V^{(th)}(f, 0) \approx 4.80 \times 10^{-14}$  V<sup>2</sup>/Hz. The detectable Johnson-Nyquist voltage noise within a bandwidth of 10 Hz should therefore be  $\sqrt{4.80 \times 10^{-14} \text{ V}^2/\text{Hz} \times 10 \text{ Hz}} \approx 0.70$   $\mu$ V.

Returning to Fig. 3(a), we realize that the rms voltage noise values reported above for both live (1.55  $\mu$ V) and dead cells (0.76  $\mu$ V) are larger than the Johnson-Nyquist noise voltage (0.70  $\mu$ V). This qualitatively suggests that “excess”  $1/f$  noise must be dominating for both live and dead bacteria. What is also remarkable and perhaps unexpected is the enhanced electrical noise of live cells as compared to dead cells. The excess  $1/f$  noise will precisely be the topic of our detailed study.

### 4. Excess noise

In order to understand the source of the excess voltage noise in the microfluidic resistor, we turn to equilibrium resistance noise. We first derive the dependence of the noise power on bias current. As shown in Fig. 2(d), the applied bias current  $I$  is divided into two,  $I_R$  through  $R_m$  and  $I_C$  through  $C_m$ , so that  $I = I_R + I_C$ . For  $I_R$ , we find  $I_R = \frac{I}{(1 + j\omega_o R_m C_m)}$ , where  $\frac{\omega_o}{2\pi} = f_o = 160$  Hz. In Fig. 2(d) the resistance noise is modeled as being generated by a time-dependent fluctuating resistance  $r(t)$  in series with  $R_m$  [24]. Under bias current  $I$ ,



the resistance fluctuations are turned into voltage fluctuations via Ohm's Law. The PSD of the excess voltage noise from the resistance fluctuations is  $\frac{I^2 S_R(f)}{1 + \omega_o^2 R_m^2 C_m^2}$ , where  $S_R(f)$  is the PSD of the resistance fluctuations in units of  $\Omega^2/\text{Hz}$ . Thus, the PSD of the current-dependent excess voltage noise measured between the nodes *A* and *B* in Fig. 2(d) can be expressed as

$$\begin{aligned} S_V^{(\text{ex})}(f, I) &= I^2 S_R(f) \left[ \frac{|Z_{\text{in}}|^2}{(1 + \omega_o^2 R_m^2 C_m^2)^2 |Z_m + Z_{\text{in}}|^2} \right] \\ &= I^2 S_R(f) \mathcal{C}. \end{aligned} \quad (2)$$

Here the factor  $\mathcal{C}$  is a dimensionless coefficient that quantifies how the noise generated in the microfluidic resistor is attenuated at the output. In our experiments, the factor  $\mathcal{C}$  is assumed to be only a function of  $R_m$ , since  $Z_{\text{in}}$  and the capacitance  $C_m$  coming mostly from the wiring stay constant. The value of  $R_m$  changes with the number  $N$  of bacteria in the microchannel and/or the resistivity of the different electrolytes. Using the circuit parameters given above, i.e.,  $C_m$ ,  $Z_{\text{in}}$ , and  $\omega_o$ , we can readily determine  $\mathcal{C}$  as a function of  $R_m$  as shown in Appendix C.

In the experiments, we measure the total voltage noise PSD as

$$\begin{aligned} S_V^{(\text{tot})}(f) &= S_V^{(\text{ex})}(f, I) + S_V^{(\text{th})}(f, 0) \\ &= \mathcal{C}(R_m) I^2 S_R(f) + 4k_B T R_n. \end{aligned} \quad (3)$$

When comparing measurements with different  $R_m$  values, it is thus necessary to deconvolute the effects of  $R_m$  from the measured noise for consistency. This should be the case, for instance, when comparing data taken in different electrolytes or when the noise power is measured as a function of number  $N$  of bacteria in the microchannels. In previous work, we have established that the  $R_m$  value depends on  $N$  approximately linearly as  $R_m(N) \approx 2.5 \text{ M}\Omega + N \times 2.5 \text{ k}\Omega$  for *K. pneumoniae* and as  $R_m(N) \approx 2.5 \text{ M}\Omega + N \times 3.5 \text{ k}\Omega$  for *S. saprophyticus* [25]. To compare noise measurements, one should first subtract from a given  $S_V^{(\text{tot})}(f)$  data the thermal noise contribution  $S_V^{(\text{th})}(f, 0)$ . Then by using the  $\mathcal{C}(R_m)$  corresponding to the  $R_m$  value of the microfluidic resistor, one can obtain the PSD of the resistance fluctuations as

$$S_R(f) = \frac{S_V^{(\text{tot})}(f) - S_V^{(\text{th})}(f, 0)}{I^2 \mathcal{C}(R_m)}. \quad (4)$$

The so-called normalized PSD  $S(f)$  can then be calculated as [37]

$$\begin{aligned} S(f) &= \frac{S_R(f)}{R_m^2} \\ &= \frac{S_V^{(\text{tot})}(f) - S_V^{(\text{th})}(f, 0)}{\mathcal{C}(R_m) I^2 R_m^2}. \end{aligned} \quad (5)$$

### C. Data analysis

#### 1. Basic steps

To recapitulate, we measure the voltage noise,  $v(t)$ , in time domain as a function of the bias current  $I$ . We now describe how these data are processed. Figure 4(a) shows representative data traces from our measurements of live *K.*

*pneumoniae* in LB under different bias currents  $I$ , with  $I$  as indicated in the figure. The data are first numerically filtered such that the remaining fluctuations are in the frequency range of  $0.05 \text{ Hz} \leq f \leq 10 \text{ Hz}$ . As seen in the data traces in Fig. 4(a), we measure  $v(t)$  over a period of 3 min for each applied  $I$ . These 3 min traces are thus long enough that various artifacts can be removed consistently but short enough that bacteria do not grow substantially and divide. The artifacts arise because bacteria may randomly enter into or escape from the microchannels; these excursions by bacteria can generate spikes [e.g., Fig. 4(a), center and right insets]. Although rare, these artifacts can change the characteristics of the noise data. We thus remove these spikes from the measured  $v(t)$  traces before we calculate the frequency domain PSDs. In summary, we use a 2-min-long portion of the  $v(t)$  data to calculate the PSDs,  $S_V^{(\text{tot})}(f)$ . The PSD is calculated by taking a fast Fourier transform (FFT) of the autocorrelation function of a 2-min-long  $v(t)$  data trace. The PSDs [Fig. 4(b)] are then smoothed [Fig. 4(c)] using an eight-point moving average [40–42]. To analyze the asymptotic low-frequency behavior of the excess noise, we calculate the normalized PSD,  $S(f)$ , of the excess noise. For this, we first determine  $S(f)$  for each  $I$  using Eq. (5). We then find the average value of  $S(f)$  [28,43]. The small symbols in Fig. 4(d) show  $S(f)$  calculated from  $S_V^{(\text{tot})}(f)$  at different  $I$  values, and the large symbols show the average  $S(f)$ .

#### 2. Averaged excess noise

Finally, we also analyze the dependence of the excess voltage noise on  $I$ ,  $\Delta p$ , and  $N$  below. To this end, we select a frequency range, where  $S_V^{(\text{tot})}(f)$  is significantly above the white (thermal) noise level and determine the PSD of the excess noise from Eq. (3), i.e.,  $S_V^{(\text{ex})}(f) = S_V^{(\text{tot})}(f) - S_V^{(\text{th})}(f, 0)$ . Here the PSD of the thermal noise,  $S_V^{(\text{th})}(f, 0)$ , is assumed to be frequency independent. We then average the excess noise over this frequency range as [44,45]

$$\overline{S_V^{(\text{ex})}(f)} = \frac{1}{f_1 - f_2} \int_{f_1}^{f_2} S_V^{(\text{ex})}(f) df. \quad (6)$$

The frequency band we use for these averages is 0.05–0.2 Hz.

### D. Control experiments

In a number of additional measurements, we have characterized the noise in the microchannels without any bacteria. In these experiments, the microchannels are filled with just the electrolyte solutions, LB and PBS. Some experiments are repeated at 23 °C. The measurements of the electrolytes without bacteria are performed with fresh buffers. The experimental approach and data analysis steps are identical to those above.

## III. RESULTS

We first make observations on the frequency domain characteristics of the measured noise. These observations lead us to the conclusion that the noise is due to equilibrium resistance fluctuations. We then show the scaling behavior of the measured noise by obtaining its normalized PSD  $S(f)$ .

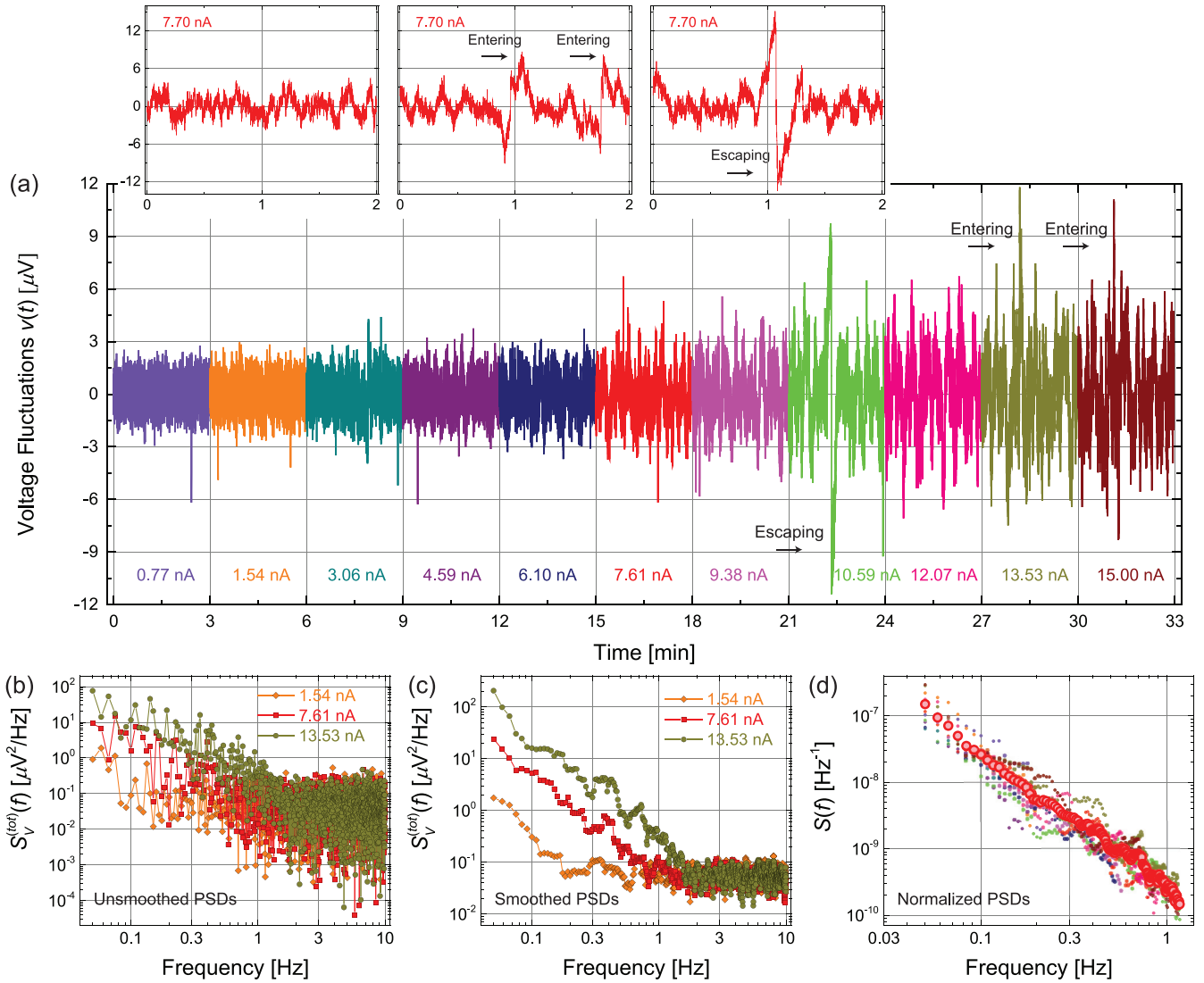


FIG. 4. (a) Representative time domain  $v(t)$  traces from measurements on live *K. pneumoniae* in LB at  $37^\circ\text{C}$  under different bias currents  $0.77 \text{ nA} \leq I \leq 15.00 \text{ nA}$  with  $N \approx 300 \pm 50$  and  $\Delta p \approx 0.6 \text{ kPa}$ . The rms values of  $I$  are as indicated in the figure. Upper insets show examples of  $v(t)$  measured at  $I \approx 7.70 \text{ nA}$ , with no artifacts (left), with two bacteria entering the microchannel (center), and with one bacterium escaping from the microchannel (right)—as observed in microscope images. The arrows indicate the instants when the bacteria enter and escape. (b) Representative PSDs  $S_V^{(\text{tot})}(f)$  of  $v(t)$  for three different  $I$  values before and (c) after smoothing. (d) Normalized PSDs  $S(f)$  of excess noise. The data show  $S(f)$  for each  $I$  (small symbols) and average of  $S(f)$  over  $I$  (large symbols).

## A. Noise PSD as a function of different parameters

### 1. Bias current

Figure 5(a) shows the PSDs of the voltage fluctuations,  $S_V^{(\text{tot})}(f)$ , measured in microchannels filled with  $N \approx 300 \pm 50$  live and dead cells at different bias current values. All the PSDs are obtained from time domain data, such as those in Fig. 4 using the steps described in Sec. II C. As noted above, the time domain data traces do not contain any voltage spikes due to large perturbations, such as bacterial divisions or displacements. Several observations are noteworthy in Fig. 5(a). For each  $I$ , the PSD exhibits a well-defined frequency  $f_w$ , where the behavior of the curve changes. For  $f > f_w$ , the spectrum is white and independent of  $I$ ; the experimentally measured white noise PSD of  $5.25 \times 10^{-14} \text{ V}^2/\text{Hz}$  is con-

sistent with the amplifier input noise combined with the Johnson-Nyquist noise of the microfluidic device, which we have estimated above in Sec. II B to be  $4.80 \times 10^{-14} \text{ V}^2/\text{Hz}$ . For  $f < f_w$ , the PSDs increase as frequency decreases, showing typical  $1/f$  excess noise characteristics [46] for both live and dead cells. The value of  $f_w$  also appears to increase with  $I$ .

We now turn to the dependence of the excess noise on  $I$ . Here we compare  $\overline{S_V^{(\text{ex})}(f)}$  values, as defined in Eq. (6) above, for different  $I$  [44,45]. Figure 5(b) shows  $\overline{S_V^{(\text{ex})}(f)}$  as a function of  $I$ . For live cells, the  $\overline{S_V^{(\text{ex})}(f)}$  data can be fitted to a quadratic function as  $\overline{S_V^{(\text{ex})}(f)} \approx \Gamma_l I^2$ , with  $\Gamma_l \approx 1.15 \times 10^5 \Omega^2/\text{Hz}$ . The noise of dead bacteria in Fig. 5(b) can also

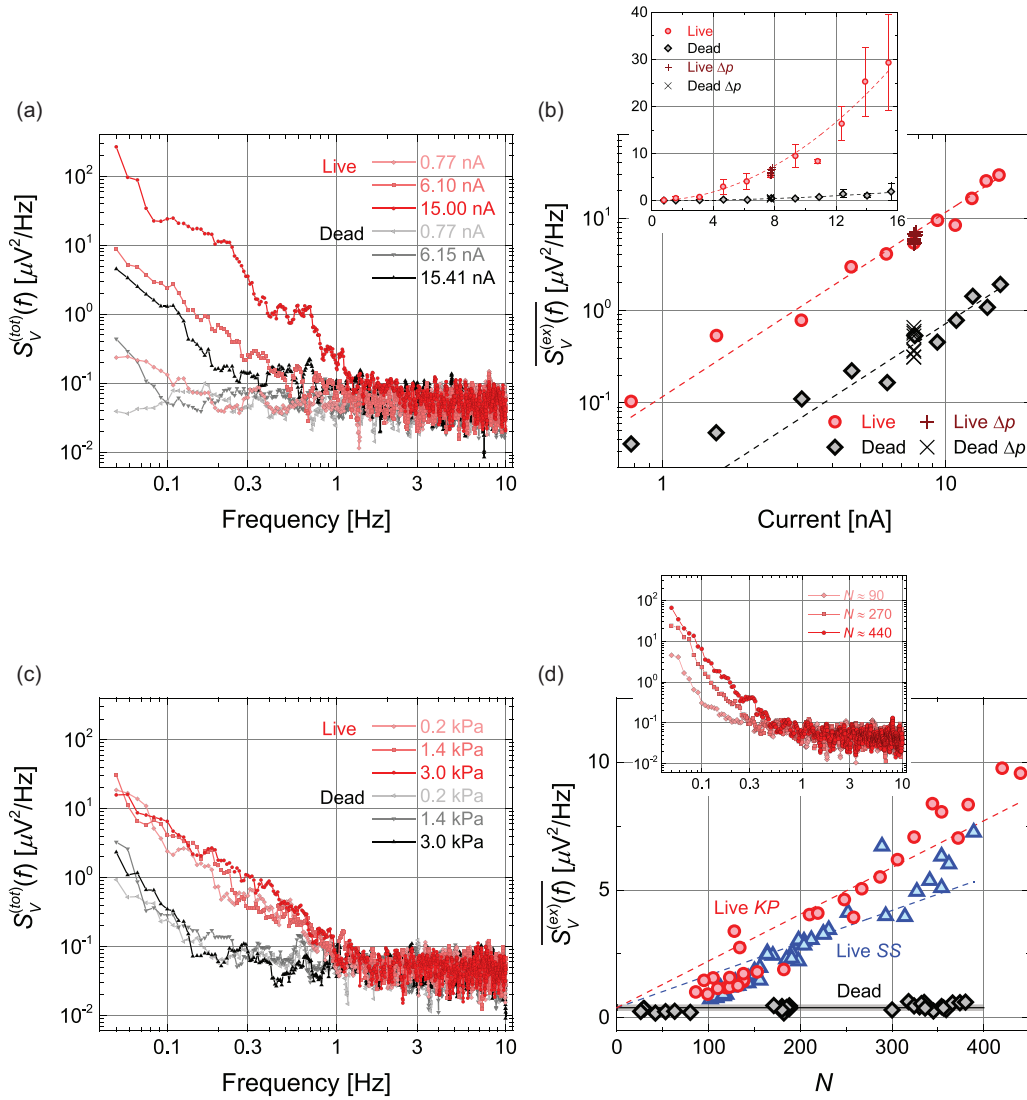


FIG. 5. (a) Voltage noise PSDs  $S_V^{(\text{tot})}(f)$  for different bias  $I$  for live and dead (*K. pneumoniae*) cells. There are approximately  $300 \pm 50$  cells in both devices, and  $R_m$  values are similar. (b) Averaged PSD  $S_V^{(\text{ex})}(f)$  of the excess voltage noise as a function of  $I$ . Each data point is the average from three independent experiments with nominally identical devices that have  $300 \pm 50$  cells and similar  $R_m$  values. The dashed lines are quadratic fits of the form  $S_V^{(\text{ex})}(f) = \Gamma I^2$ , with  $\Gamma = 1.16 \times 10^5 \Omega^2/\text{Hz}$  (live) and  $7.21 \times 10^3 \Omega^2/\text{Hz}$  (dead). The symbols + and  $\times$ , respectively, show  $S_V^{(\text{ex})}(f)$  for live and dead cells at different  $\Delta p$  ranging from 0.2 kPa to 3.0 kPa with an increment of 0.4 kPa under  $I \approx 7.75$  nA. Inset shows the same data on a linear scale; error bars show single standard deviations. (c) Representative  $S_V^{(\text{tot})}(f)$  for live and dead cells at three different  $\Delta p$  values, with  $I \approx 7.75$  nA. (d) Averaged PSD  $S_V^{(\text{ex})}(f)$  as a function of number  $N$  of cells in the microchannels. The bias current is  $I \approx 7.75$  nA for all. Each data set consists of data points from at least three independent experiments. The line parallel to the  $x$  axis corresponds to the excess noise power within the 0.2 Hz bandwidth for dead cells. The dashed lines are linear fits with the  $y$  intercepts fixed to the excess noise value for the dead cells. Inset shows three representative  $S_V^{(\text{tot})}(f)$  curves for live *K. pneumoniae* cells with different  $N$  taken using the same bias  $I \approx 7.78$  nA.

be fitted to a quadratic function,  $\Gamma_d I^2$ —at least for the high current region of the data with  $\Gamma_d \approx 7.20 \times 10^3 \Omega^2/\text{Hz}$ . The dashed lines in Fig. 5(b) show the quadratic fits. It is important to emphasize that all the data here are consistently taken on  $N \approx 300 \pm 50$  cells, and all  $R_m$  values remain in the range  $R_m \approx 3.10 \pm 0.40 \text{ M}\Omega$ .

Two important conclusions can be made based on the data and fits in Fig. 5(b). The  $I^2$  dependence of the excess noise suggests that, in both cases, the noise is induced by “equilibrium” resistance fluctuations [26–30]. Live cells exhibit a significantly higher amplitude than dead ones with

$\Gamma_l \gg \Gamma_d$ , indicating that noise generation is linked to bacterial metabolism. The origin of the noise from dead cells is not entirely clear and will be further addressed in Sec. III B below.

## 2. Hydrodynamic pressure

Figure 5(c) shows  $S_V^{(\text{tot})}(f)$  for different applied pressures  $\Delta p$  across the channel at a fixed bias of  $I \approx 7.75$  nA. The measured noise remains independent of  $\Delta p$ , and hence the bulk flow velocity, as  $\Delta p$  is varied by more than an order of magnitude. We further note that  $S_V^{(\text{ex})}(f)$  at  $I \approx 7.75$  nA exhibits no dependence on  $\Delta p$  [Fig. 5(b)].

During the experiments, we establish a net flow from the inlet to the outlet. The drag force due to this steady flow has a stabilizing effect on the system, with the bacteria snugly jammed in the microchannel toward the nanoconstriction. The electrokinetic and other flow forces in the system do not move the bacteria due to the presence of this net steady flow from the inlet toward the nanoscale constriction. Appendix D provides more details on the control experiments where we measure the hydrodynamic and electrokinetic forces on the bacteria in our system.

### 3. Number of cells

We next demonstrate how the number  $N$  of cells in the microchannel affects the measured noise characteristics. We increase the number of bacteria in the microchannels via growth for live cells and via trapping from flow for dead cells. We measure  $v(t)$  at fixed  $I \approx 7.75$  nA as a function of  $N$ . The inset of Fig. 5(d) shows  $S_V^{(\text{tot})}(f)$  of live cells for three different  $N$  values, with the PSD increasing with  $N$  in the low-frequency region. The main plot in Fig. 5(d) shows  $S_V^{(\text{ex})}(f)$  as a function of  $N$  obtained from many different data traces such as those in the inset. While  $S_V^{(\text{ex})}(f)$  increases monotonically with  $N$  for live cells, it remains at a constant value (solid line) for dead cells. The increase of  $S_V^{(\text{ex})}(f)$  with  $N$  for live cells indicates that the noise powers from individual cells are additive. The noise power of *K. pneumoniae* appears to be slightly larger than that of *S. saprophyticus*. We note that, since  $R_m$  increases with  $N$ , the fraction of the noise power that is coupled to the amplifier changes with  $N$ . Thus, the data provide only a qualitative picture.

## B. Normalized PSD of the excess noise

### 1. Excess noise of live bacteria

The  $I^2$  dependence observed in Fig. 5(b) suggests that the noise is due to equilibrium resistance fluctuations. To analyze the asymptotic low-frequency behavior of the excess noise, we return to Eq. (5) and calculate the normalized PSD,  $S(f)$ , of the excess noise. Normalizing the data this way removes the contribution of the thermal noise and all the  $I$  and  $R_m$  dependences. The data with different bias currents should then collapse onto a single curve [47].  $S(f)$  of different systems, e.g., dead and live bacteria, can then be directly compared.

The collapsed  $S(f)$  data are shown in Fig. 6(a) for *K. pneumoniae* and in Fig. 6(b) for *S. saprophyticus*, in both LB and PBS. For live bacteria in LB,  $S(f) \propto Af^{-2}$ . The noise of live cells in PBS is noticeably lower than that in LB. In all these measurements,  $N \approx 300 \pm 50$ .

### 2. Excess noise of dead bacteria and electrolytes

The black data traces in Figs. 6(a) and 6(b) show the average  $S(f)$  for dead *K. pneumoniae* and dead *S. saprophyticus*, respectively, with the shaded regions corresponding to the error (single standard deviations). For dead bacteria,  $S(f) \propto Bf^{-3/2}$ .

Microchannels filled with electrolytes (either LB or PBS) with no cells at both 37 °C and 23 °C show the same noise characteristics and levels as microchannels filled with dead

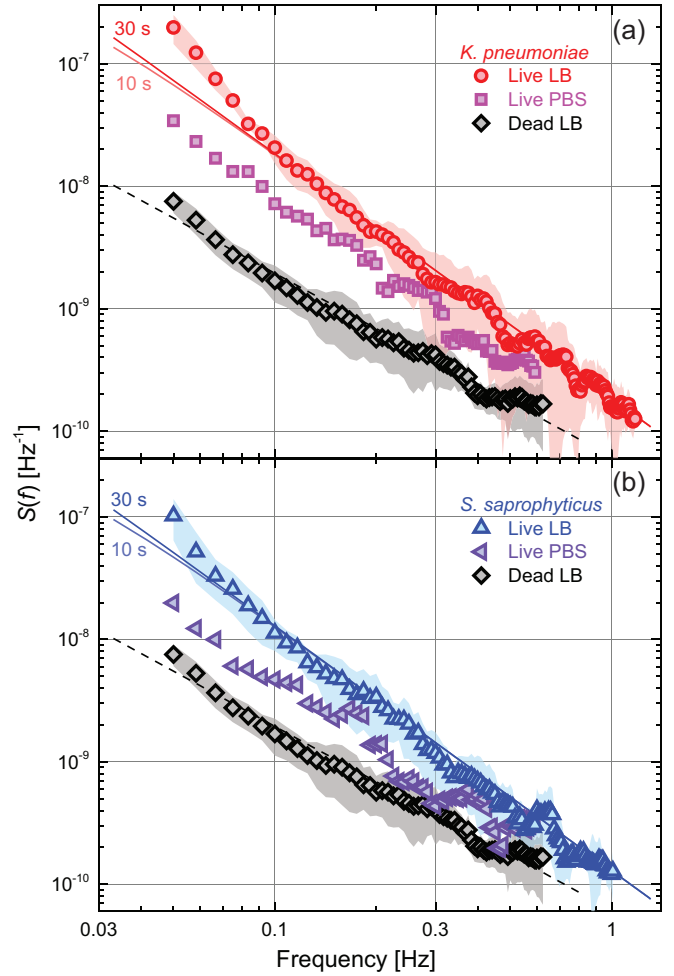


FIG. 6. Collapse and scaling of the noise data. Normalized PSDs,  $S(f)$ , of resistance fluctuations for live *K. pneumoniae* (a) and *S. saprophyticus* (b) in LB and PBS. The black data trace in each plot shows the average  $S(f)$  for dead *K. pneumoniae* in LB and dead *S. saprophyticus* in LB. The shaded regions show the error (single standard deviations). Each data trace on live and dead cells in LB are obtained from three independent experiments. The data trace on live cells in PBS is from a single experiment. The black dashed lines are  $S(f) = B/f^\beta$ , with  $B = 6.15 \times 10^{-11}$  and  $\beta = 1.50$ . The solid lines are fits to  $S(f) = \frac{At^2}{1+4\pi^2 f^2 \tau^2}$  using  $\tau = 10$  s and 30 s for *K. pneumoniae* (red) and *S. saprophyticus* (blue); the  $A$  values for both time constants for *K. pneumoniae* and *S. saprophyticus* are approximately  $7.30 \times 10^{-9}$  and  $5.10 \times 10^{-9}$ , respectively.

bacteria. This can be seen clearly in the collapsed average  $S(f)$  data in Fig. 7.  $S(f)$  curves in Fig. 7 for no bacteria and dead bacteria also follow the same scaling behavior. In order to obtain these collapse plots, we follow the steps described above in Sec. II C 1 and use  $\mathcal{C}(R_m)$  to correct the measured noise in different electrolytes. This is because the electrical conductance values, and hence the  $R_m$  values, for these devices differ significantly: at 37 °C, the  $R_m$  values for devices filled with LB and PBS are 2.5 M $\Omega$  and 1.7 M $\Omega$ , respectively; at room temperature (23 °C), the  $R_m$  value for LB is 3.0 M $\Omega$ ; the electrical conductivity of PBS at 37 °C, LB at 37 °C, and LB at 23 °C are approximately 1.47 S/m, 1.00 S/m, and



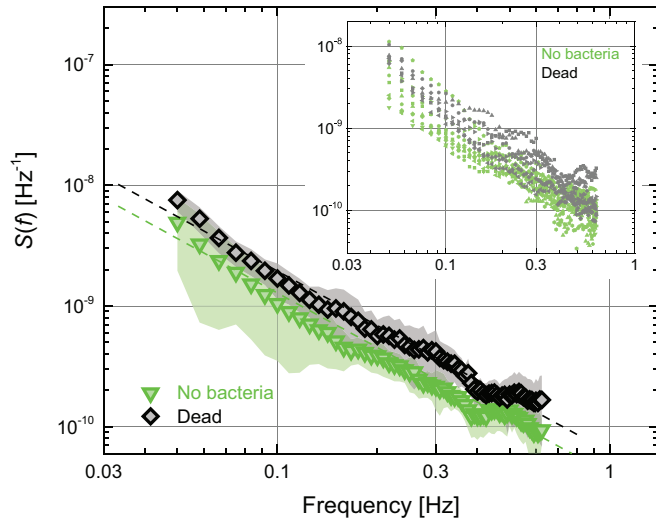


FIG. 7. Normalized PSD  $S(f)$  of the resistance fluctuations for electrolytes containing no bacteria and dead bacteria. The large symbols show the average values of the experiments with just the electrolyte (green) and with dead bacteria (black); the shaded regions show the error (single standard deviations); the dashed lines are not fits but show the asymptotic behavior and correspond to  $S(f) = B/f^\beta$ , with  $B = 4.05 \times 10^{-11}$  and  $\beta = 1.50$  for no bacteria (green) and  $B = 6.15 \times 10^{-11}$  and  $\beta = 1.50$  for dead bacteria (black). The inset shows the data sets from independent experiments; the green symbols correspond to data from nine independent experiments, three with PBS at 37 °C, three with LB at 37 °C, and three with LB at 23 °C; the gray symbols show data from six independent experiments three with dead *K. pneumoniae* and three with dead *S. saprophyticus*, both in LB at 37 °C.

0.83 S/m, respectively. These conductivity values agree with those reported in the literature [48–50].

In summary, the presence or absence of dead cells in the electrolyte does not change the background noise appreciably; nor does interchanging LB with PBS or decreasing the temperature to 23 °C. More details are available in the Supplemental Material [51]. It may therefore be justifiable to collapse all the background data onto a single curve. All these suggest that the background noise is due to an intrinsic bulk process in the electrolyte—although we cannot conclusively rule out other possibilities, such as contact noise [52] or extrinsic noise.

#### IV. DISCUSSION

We first systematically look at possible artifacts, concomitants, and perturbations that may give rise to the observed noise. These include extrinsic noise, measurement artifacts, bacterial movements, flow forces, electrokinetic forces, electrical perturbations, and Joule heating. For each case, we provide estimates or experimental evidence that suggests that the noise does not come from this particular source. (Some of the details are presented in the Appendices.) We then return to our hypothesis that bacterial metabolism is responsible for the observed noise and provide some theoretical support to our experimental observations.

#### A. Possible artifacts

We first consider possible artifacts and perturbations that might give rise to the observed excess noise. The fact that we can directly compare results on live and dead cells has convinced us that our measurements are not dominated by extrinsic noise. Our microchannel device is, in principle, capable of transducing bacterial movements into resistance fluctuations [53]. We can rule out any inherent rigid body movements of live bacteria (e.g., wiggling) as a noise source because our bacteria are highly nonmotile. The steady flow and the electrokinetic flows due to applied fields in the microchannel can also excite and sustain rigid body movements [54]. However, this cannot be the source of the observed noise simply because fixed cells would show the same level of noise (e.g., Fig. 2). Detailed measurements described in Appendix D indicate that electrokinetic forces are negligible compared to the steady drag force of the pressure-driven flow, which pushes the bacteria toward the nanoconstriction and jams them. We also investigate a possible temperature increase due to Joule heating and conclude that the increase is negligible. An applied electric field, i.e., the bias, can perturb the bacterial membrane and its proteins [55–57], changing the influx and efflux rates. Our electric field strength is too small to induce any electrical perturbations, and bacteria appear to grow normally in our microchannels during our measurements. We therefore conclude that the observed noise is rooted in bacterial metabolism.

#### B. Nanomechanical fluctuations of bacteria

Active random oscillations and movements are commonly observed in many microorganisms and cells [58–65]. Due to active biochemical processes in the cytoplasm and cell membrane [66,67], highly nonmotile bacteria are also expected to exhibit random nanomechanical oscillations. During these nanomechanical oscillations, the bacteria go through quasi periodic deformations, which in principle could get converted to electrical noise by our microchannel transducer [53].

In order to get an order of magnitude estimate of nanomechanical fluctuations, we convert the observed electrical noise power into an active effective temperature  $T_{\text{eff}}$  for the bacteria. To this end, we first numerically calculate the rms thermal amplitude, i.e., nanomechanical thermal equilibrium noise, of a bacterium in several of its eigenmodes; we then convert the nanomechanical noise into electrical resistance noise by considering the change in the geometric cross section of the microchannel due to the random deformations of 300 bacteria. Based on the responsivity of our microchannel transducer, the random thermal oscillations of 300 bacteria at the equilibrium temperature of 310 K (37 °C) result in resistance noise with an rms value of  $\sim 0.8 \Omega$ . Experimentally measured rms resistance noise, on the other hand, is  $\sim 200 \Omega$ . To match the observed noise levels, we estimate that a bacterium ought to attain an effective temperature of  $T_{\text{eff}} \sim 10^7 \text{K}$ . While an active system such as a bacterium should have  $T_{\text{eff}} > 310 \text{K}$  [58–60,64], this level of activity seems unreasonable. Nanomechanical motion of bacteria is thus an unlikely source for our observations. Details of the simulations, the assumptions made,

and a thorough discussion of the results are provided in Appendix D.

### C. Charge noise model

Our hypothesis is that the source of the fluctuations is electrical. The electrolyte-filled microchannels can be considered as one-dimensional conductors in which the primary charge carriers are  $\text{Na}^+$  and  $\text{Cl}^-$  ions. Each microchannel is assumed to be long and uniformly filled with bacteria (i.e.,  $N \approx 300$ ). Monovalent ions, such as  $\text{K}^+$ ,  $\text{Na}^+$ , and  $\text{Cl}^-$ , move into and out of the bacteria randomly; this causes fluctuations in the number of charged carriers within the conductors and hence resistance noise.

We first construct an electrical noise model of a single cell by assuming that the flux of a certain ion X into or out of the cell is proportional to the number of ions within the cell. For instance, if there are excess  $\text{Na}^+$  ions in the cell,  $\text{Na}^+$  ions will be transported out of the cell and vice versa. This is expected because the excess  $\text{Na}^+$  in the cell will change the Nernst potential for  $\text{Na}^+$  and activate the ion channel conduction in one direction. Thus, for any given ion X,

$$\frac{dn_X}{dt} = -\phi(n_X), \quad (7)$$

where  $n_X$  is the total number of intracellular X ions and  $\phi$  is the rate of transport of X ions through the cell membrane as a function of  $n_X$ . The minus sign indicates that when intracellular value of  $n_X$  is decreasing the  $n_X$  flux is positive. Expanding around the equilibrium value  $n_X = \bar{n}_X + \Delta n_X$ , we write

$$\frac{d\Delta n_X}{dt} = -\frac{\Delta n_X}{\tau_X} + \xi_X, \quad (8)$$

with  $\xi_X$  being a white noise term. Here  $\phi(\bar{n}_X) = 0$ , and  $\tau_X = \left(\frac{\partial \phi}{\partial n_X}\bigg|_{\bar{n}_X}\right)^{-1}$  can be regarded as a lifetime for ions or the relaxation time for an ionic perturbation within the cell. From this, we find [68,69]

$$S_{n_X}(f) = \frac{4\overline{(\Delta n_X)^2}\tau_X}{1 + 4\pi^2 f^2 \tau_X^2} \quad (9)$$

for the PSD for the fluctuations of the number  $n_X$  of intracellular ions of type X in a single bacterium. Since we are interested in estimating an order of magnitude, we assume that the  $\tau_X$  for different ions are roughly equal and define an overall effective time constant  $\tau$  such that  $\tau \sim \tau_X$ . We also assume that the noise powers generated by bacteria are additive. Then the PSD of the fluctuations in the total number of charge carriers within our microfluidic resistor containing many bacteria should be expressible in the form

$$S_n(f) = \frac{4\overline{(\Delta n)^2}\tau}{1 + 4\pi^2 f^2 \tau^2}, \quad (10)$$

where  $\overline{(\Delta n)^2}^{1/2} = \Delta n_{rms}$  is the rms value of the fluctuations in the number of charge carriers. Note that the particle flux at

equilibrium is assumed to be zero—as opposed to the case in generation recombination noise in semiconductors [68].

For the equivalent microfluidic resistor  $R_m$  (with ten microchannels), the relationship between the PSD of the resistance fluctuations,  $S_R(f)$ , and the PSD of the carrier number fluctuations,  $S_n(f)$ , is [69]

$$S(f) = \frac{S_R(f)}{R_m^2} = \frac{S_n(f)}{n^2}. \quad (11)$$

Here  $n$  is the total number of charge carriers in the resistor. Under the assumption of spatial uniformity, Eq. (11) holds for a single microchannel (out of the ten) (see Appendix E), which has  $n \approx 4 \times 10^{10}$  at the 85 mM NaCl concentration of LB. Thus, there are  $n \pm \Delta n_{rms}$  charge carriers within the LB filling the microchannel due to the noise generated by bacteria.

We do not see the corner frequency in our data and thus cannot determine  $\tau$  from our experiments. We turn to previous work [14] for an approximate value of  $\tau$ . In this remarkable paper [14], the autocorrelation functions of spontaneous electrical blinks from single bacterial cells were shown to decay exponentially over a period of 10–30 s. This suggests that bacterial membrane potentials and the intracellular ion concentrations relax with a time constant  $10 \text{ s} \lesssim \tau \lesssim 30 \text{ s}$ . For 10 s and 30 s, we obtain the fits shown in Fig. 6 with  $\overline{(\Delta n)^2} \sim 5 \times 10^{13}$  for 30 cells at equilibrium yielding  $\Delta n_{rms}^{(1)} \sim 1.3 \times 10^6$  per cell. We have estimated the other relevant time constants in the system due to flow, drift and diffusion, and found that the diffusion time constant in the system is close to 10 s. It is also noteworthy that the noise data in Fig. 6 start to deviate from the  $1/f^2$  asymptote below 0.06 Hz, suggesting that another noise process might be dominating at our lowest frequencies.

### D. Estimation of the membrane potential noise

To estimate the noise in the membrane potential due to the charge noise, we use two approaches.

In the first, we assume that the noise in the transmembrane ionic current results in fluctuations in the total charge in close proximity of the membrane, i.e., on the plates of the capacitor in the circuit in Fig. 1(a). Then  $e_n \sim \frac{e\Delta n_{rms}^{(1)}}{C} \approx 3.5 \text{ V}$ , with  $\Delta n_{rms}^{(1)} \approx 1.3 \times 10^6$ ,  $C \approx 6 \times 10^{-14} \text{ F}$ , and  $e \approx 1.60 \times 10^{-19} \text{ C}$  [12] with  $C$  being the membrane capacitance of the cell.

In the second, we estimate  $e_n$  from fluctuations in the intracellular ion concentrations. We assume that the ions are distributed uniformly inside (and outside) the cell and that only  $\text{K}^+$ ,  $\text{Na}^+$ , and  $\text{Cl}^-$  ions contribute to the steady-state value of  $V_{mem}$ . We find the change in the membrane potential with respect to each ion concentration from the Goldman-Hodgkin-Katz equation [12] and find the total rms change by adding each contribution as

$$e_n \approx \frac{RT}{F} \left( \frac{(p_K \Delta[\text{K}^+]_i)^2 + (p_{Na} \Delta[\text{Na}^+]_i)^2}{(p_K [\text{K}^+]_i + p_{Na} [\text{Na}^+]_i + p_{Cl} [\text{Cl}^-]_o)^2} + \frac{(p_{Cl} \Delta[\text{Cl}^-]_i)^2}{(p_K [\text{K}^+]_o + p_{Na} [\text{Na}^+]_o + p_{Cl} [\text{Cl}^-]_i)^2} \right)^{1/2}, \quad (12)$$

where  $R$  is the universal gas constant,  $T$  is the temperature,  $F$  is Faraday's constant;  $p_X$  is the relative membrane permeability, and  $[X]_i$  and  $[X]_o$  are the uniform intracellular and extracellular concentrations of the ion. The rms fluctuations in intracellular ion concentration for each ion is estimated to be of order,  $\Delta[X]_i \sim \frac{\Delta n_i^{(1)}}{V_b} \sim 10^{24} \text{ m}^{-3}$ , for a cell with volume  $V_b \sim 10^{-18} \text{ m}^3$  [12]. The extracellular ion concentrations are assumed to remain constant. By substituting the  $\Delta[X]_i$  values along with the values of  $p_X$ ,  $[X]_i$ , and  $[X]_o$  into Eq. (12), we find  $e_n \sim 1.3 \text{ mV}$ . More details are available in Appendix E 2.

These two extreme values for the membrane potential fluctuations, i.e., 1.3 mV and 3.5 V, suggest that the fluctuations depend strongly upon how nonuniformities in ion concentrations get dissipated within the ‘‘crowded environment’’ of the cell. We estimate that an ion would probably diffuse a distance equal to the length scale of a bacterium in  $\sim 10 \text{ ms}$  [70]. This indicates that a more accurate noise model for the membrane potential and the electrical fluctuations of the entire bacterium should take into account intracellular diffusion.

## V. CONCLUSIONS

Our measurements represent a significant step in understanding the role of fluctuations in bacterial ion homeostasis. By carrying out electrical noise measurements on live and dead bacteria, we have shown evidence that the charge state of live bacteria fluctuates over time. A direct consequence of this observation is that intracellular ion concentrations and the membrane potential  $V_{\text{mem}}$  both have strongly fluctuating components. It is well established that  $V_{\text{mem}}$  and intracellular ion concentrations in bacteria affect a number of cellular processes in a crucial manner. Among these processes are ATP synthesis [6], cell division [7], cell motility [71], antibiotic resistance [8], environmental sensing [3,4], and electrical communication between cells [5,72]. It is thus reasonable to expect that  $V_{\text{mem}}$  and the intracellular ion concentrations should practically remain constant over time, because drastic changes and large fluctuations in  $V_{\text{mem}}$  and ion concentrations would strongly perturb all the above-mentioned cellular processes. More and more experiments, including ours, suggest that the ionic makeup of the cell, and hence  $V_{\text{mem}}$ , fluctuates strongly. It remains to be seen whether bacteria utilize these fluctuations to its advantage or whether there are built in mechanisms of noise evasion.

We have also established time-resolved electrical resistance measurements as a sensitive tool for studying bacteria. Even lower frequencies and higher sensitivities may be achieved in future studies by redesigning the microfluidic resistor, e.g., by incorporating a nulling bridge in the design or and reducing the background fluctuations. It may also be possible, in principle, to do these experiments in larger channels with many more bacteria—provided that any bacteria movements can be suppressed. Our microfluidic resistor is designed to have a source resistance such that efficient coupling of noise can be achieved to a low-frequency high-impedance amplifier. This requirement can be circumvented, for instance, by performing the measurement at high frequency, where a larger channel with a source resistance close to  $50 \Omega$  can be used. Finally, understanding the source of the fluctuations in the electrolyte is also a problem of fundamental relevance. To this

end, one may perform experiments with different electrodes and in different electrolytes.

## ACKNOWLEDGMENTS

This work was supported by NIH (1R21AI133264-01A1). H.G. acknowledges the Boston University Nanotechnology Innovation Center BUNano Cross-Disciplinary Fellowship. The authors thank V. Yakhot and J. Tien for helpful discussions. K.L.E. discloses a potential of conflict of interest, as he is the cofounder of a company, Fluctuate Diagnostics, which aims to commercialize this technology. No potential conflicts of interest exist for Y.Y. and H.G.

## APPENDIX A: EXPERIMENTAL DETAILS

### 1. Device design and fabrication

Our microfluidic resistor is essentially a continuous polydimethylsiloxane (PDMS) microfluidic channel that is bonded onto a glass substrate with pre-patterned metallic electrodes. The device is fabricated using standard soft lithography [25]. The microfluidic channel is made up of two structures with different length scales: the large mm-scale channel narrows, at its center, to ten smaller parallel microchannels ( $l \times w \times h \approx 100 \times 2 \times 2 \mu\text{m}^3$ ). Each microchannel has a nanoconstriction ( $l \times w \times h \approx 5 \times 0.8 \times 2 \mu\text{m}^3$ ) at one end with a cross-sectional area close to that of a single bacterium. More details about the device design and fabrication can be found in [25].

### 2. Bacteria preparation

Two microorganisms, *Klebsiella pneumoniae* (ATCC 13883) and *Staphylococcus saprophyticus* (ATCC 15305), are purchased from American Type Culture Collection (ATCC, Rockville, MD). *K. pneumoniae* is a Gram-negative, non-motile, rod-shaped bacterium that has a length of 2–3  $\mu\text{m}$  and a cross-sectional area of  $0.8 \mu\text{m}^2$  [34]. *S. saprophyticus* is a Gram-positive, nonmotile, spherical bacterium that has a diameter of 1  $\mu\text{m}$  [35]. We use Luria-Bertani (LB) Lennox broth (pH 6.6; Sigma-Aldrich, St. Louis, MO) as the growth medium. The broth consists of tryptone (10 g/L), yeast extract (5 g/L) and NaCl (5 g/L). The ionic strength is  $\sim 85 \text{ mM}$ . We also use phosphate buffer saline (PBS, pH 7.4; Lonza Walkersville, Walkersville, MD) in some experiments. Details of the procedure for culturing the bacteria can be found in [25]. We measure the pH values of the media using a Pocket Pro<sup>+</sup> pH Tester (Hach, Loveland, CO) at 37 °C. The incubation of bacteria in the media does not change the pH values, and the pH values of the media remain unchanged over the entire period of our experiment ( $\sim 3 \text{ h}$ ).

To fix the cells, the following steps are used. The cells are first washed twice in PBS, the washed cells are then fixed in glutaraldehyde (Sigma-Aldrich) in LB for 2 h at 37 °C. The concentration of glutaraldehyde used is 2.5% (vol/vol) [73]. After this step, the fixed cells are washed twice in PBS and subsequently resuspended in LB for our noise measurements. Glutaraldehyde is a chemical fixative that cross-links proteins on bacterial surfaces and inhibits transport processes [36]. The fixation solution has been shown to effectively preserve

morphology of both bacterial cells and surface ultrastructures for a period longer than the duration of our experiments ( $\sim 3$  h) [73,74]. This fixation method is not expected to change the susceptibility of bacteria to electrical perturbations (see Appendix D 1).

### 3. Experimental setup

The experiments are performed on an Axio observer inverted microscope (Carl Zeiss, Oberkochen, Germany). We use a PeCon 2000-2 Temp Controller (PeCon GmbH, Erbach, Germany). At the beginning of each experiment, the sample is loaded into the microfluidic resistor under a pressure-driven flow established through the microfluidic channel using the flow controller OB1-Mk3 (Elveflow, Paris, France). More details regarding sample loading can be found in [25].

Our experiments investigate the dependence of the excess noise on three experimental parameters: the amplitude of the bias current  $I$ , the pressure gradient  $\Delta p$  of the bulk flow, and the number  $N$  of bacterial cells. When we focus on one parameter, the other two parameters are maintained more or less unchanged. Briefly, for studying the  $I$  dependence, we measure the voltage noise for  $0.70 \text{ nA} \leq I \leq 16.50 \text{ nA}$ , while keeping  $N \approx 300 \pm 50$  and  $\Delta p \approx 0.6 \text{ kPa}$ . For studying the  $\Delta p$  dependence, we measure the voltage noise under constant  $\Delta p$  in the range  $0.2 \text{ kPa} \leq \Delta p \leq 3.0 \text{ kPa}$  (incremented by  $0.4 \text{ kPa}$ ), while we keep  $I \approx 7.75 \text{ nA}$  and  $N \approx 300 \pm 50$ . For studying the  $N$  dependence, we measure the voltage noise with  $20 \lesssim N \lesssim 500$ , while maintaining  $I \approx 7.75 \text{ nA}$  and  $\Delta p \approx 0.6 \text{ kPa}$ . All measurements are performed at  $37^\circ\text{C}$ , unless indicated otherwise.

### 4. Electrical measurements and data acquisition

A SR830 DSP lock-in amplifier (Stanford Research Systems, Sunnyvale, CA) is used for the measurements. We record the output signals from the lock-in amplifier at a sampling frequency of 128 Hz using a data acquisition card NI 6221 (National Instruments, Austin, TX) through a LabVIEW (National Instruments) Virtual Instrument interface. Microscope images of the bacterial cells in the microchannels are acquired on an Axio observer inverted microscope (Carl Zeiss) with  $5\times$  and  $63\times$  objectives, an AxioCam 503 mono camera (Carl Zeiss), and ZEN image acquisition software (Carl Zeiss). Most data processing is performed using Origin (MicroCal Software, Northampton, MA).

### APPENDIX B: AUTOCORRELATION FUNCTION

In the  $1/f$  noise literature, the PSD of noise is more commonly displayed than the autocorrelation function—although there are some exceptions [75]. This is partially due to the following reason: to obtain the asymptotic  $1/f$  behavior of the noise, one needs to subtract the high-frequency white noise tail, as we have done in Sec. II C 1 [for instance, see Eq. (5) and Fig. 6]. Thus, it becomes harder to visualize asymptotic noise characteristics in the time domain. Regardless, it may be helpful to look at the autocorrelation function here for comparison.

Figure 8 shows the normalized autocorrelation functions of the voltage fluctuations,  $C_v(\Delta t) = \frac{\langle v(t)v(t+\Delta t) \rangle}{\langle v(t)^2 \rangle}$ , for different

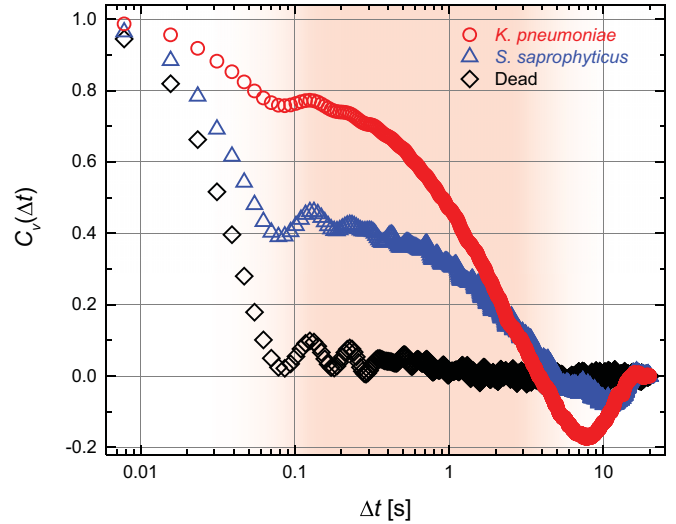


FIG. 8. Normalized temporal autocorrelation functions  $C_v(\Delta t)$  of voltage fluctuations for live *K. pneumoniae* and *S. saprophyticus* cells and background (dead cells), plotted as a function of time lag  $\Delta t$  in logarithmic scale. The shading approximately indicates the region corresponding to the frequency range shown in the PSDs in Fig. 6.

conditions. Here the angular brackets indicate averaging over time and  $\Delta t$  is the time lag. Each data trace in Fig. 8 is obtained from 12 20-s-long  $v(t)$  data traces. Briefly,  $C_v(\Delta t)$  of a single trace is computed, smoothed, and averaged.

The increase in  $C_v(\Delta t)$  at short timescales,  $\Delta t < 0.1$  s, is due to the high-frequency fluctuations, which are removed from the PSDs. At large timescales,  $\Delta t > 3$  s,  $C_v(\Delta t)$  becomes inaccurate because the data traces are only 20 s long. The dip seen in the data, in particular, may be an artifact due to the finite length of the data. The shading in Fig. 8 approximately corresponds to the frequency range of the PSDs shown in Fig. 6. The bacteria data in Fig. 8 can be fit to exponential decays with time constants of  $\sim 10$  s. In this respect, the autocorrelation function does not provide any new insight into the phenomena.

### APPENDIX C: THE DIMENSIONLESS FUNCTION $\mathcal{C}$

In Sec. III B we express the PSD of the current-dependent excess voltage noise measured between the nodes  $A$  and  $B$  in Fig. 2(b) as Eq. (2). Here the factor  $\mathcal{C}$  is a dimensionless coefficient that quantifies how the measured noise at the input of our electronics is attenuated as compared to the noise generated in the microfluidic resistor. In our experiments, the value of  $R_m$  changes with the number  $N$  of bacteria in the microchannel and/or the resistivity of the different electrolytes. The parasitic capacitance coming mostly from the wiring stays more or less constant. Thus, the factor  $\mathcal{C}$  is assumed to be only a function of  $R_m$ . Using the values given in Sec. II B for  $C_m$ ,  $Z_{in}$ , and  $\omega_o$ , we calculate  $\mathcal{C}$  as a function of  $R_m$ , as shown in Fig. 9. When comparing measurements with different  $R_m$  values, we deconvolute the effects of  $R_m$  from the measured noise for consistency by using the  $\mathcal{C}(R_m)$  corresponding to the  $R_m$  value of the microfluidic resistor, as described in Sec. II B.



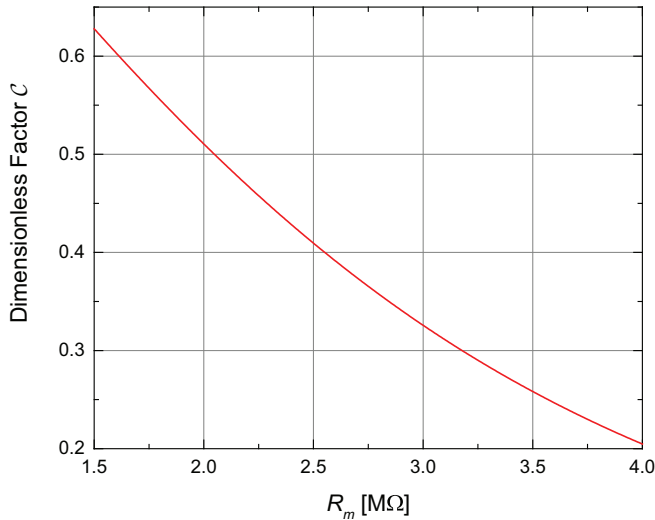


FIG. 9. The dimensionless factor  $C$  as a function of resistance  $R_m$  of the microfluidic resistor.

#### APPENDIX D: PERTURBATIONS, CONTROL EXPERIMENTS, AND VARIOUS OTHER ESTIMATES

##### 1. Electrical perturbations

At the frequency of the excitation current  $f_o = 160$  Hz, the expected change in membrane potential  $\Delta\Psi$  due to the applied electric field  $E(f_o)$  can be calculated using the Schwan equation

$$\Delta\Psi = \frac{1.5aE(f_o)}{\sqrt{1 + (2\pi f_o T)^2}}. \quad (\text{D1})$$

Here  $a$  is the radius of the bacterium and  $T$  the relaxation time of the membrane [76,77]. For a rodlike bacterium like *K. pneumoniae*, we can approximate  $a \approx 1 \mu\text{m}$  and  $2\pi f_o T \ll 1$  [56]. The highest electric field in our experiment,  $E(f_o) = 350$  V/m, corresponds to fluctuations in membrane potential of  $\Delta\Psi_{rms} = 0.52$  mV. Thus, electroporation of the bacteria membrane as well as stimulation of any voltage-gated ion channels are unlikely [55–57]. The largest current density in our experiments ( $580$  A/m<sup>2</sup>) is also expected to have no harmful effects on the bacteria [78,79].

##### 2. Electrokinetic and flow forces on a bacterium

Here we compare the magnitude of the various forces acting on the bacteria in the microchannels. In particular, bacteria experience an electrokinetic force induced by the oscillating voltage and a hydrodynamic drag force due to the pressure driven flow. Since these nonmotile bacteria are in the Stokes flow regime, estimating the flow velocities will be sufficient to assess the magnitude of the forces. We thus look at the pressure-driven component,  $u_{\Delta p}$ , and the electrokinetic component,  $u_{EK}$ , of the flow velocity in the microchannel in separate control experiments.

The pressure-driven velocity  $u_{\Delta p}$  at  $\Delta p \approx 0.6$  kPa can be estimated through optical tracking. During an experiment with live bacteria, bacteria entering the microchannels are optically tracked, as shown in Fig. 10(a). We use ImageJ [80] to analyze the videos which have a frame rate of 10 fps and a resolution of  $\pm 200$  nm. Each bacterium is tracked from the moment it enters the microchannel until its collision with the bacteria already trapped by the nanoconstriction [Fig. 10(a)]. The velocity is obtained by a linear fit of the position over time as shown in Fig. 10(b). The velocity depends on the number  $N_1$  of bacteria already trapped in the microchannel [Fig. 10(c)], because each bacterium trapped in the microchannel increases the hydraulic resistance of the microchannel. A microchannel gets completely filled with bacteria when  $N_1 \approx 40$ . During the experiments, about 300–350 bacteria are trapped in all ten microchannels. From Fig. 10(c), we estimate the steady-state flow velocity during electrical noise measurements to be  $u_{\Delta p} \approx 2.5 \mu\text{m/s}$ .

The electrokinetic flow velocity is measured in separate experiments by tracking the sinusoidal displacements of single live and dead bacteria at various carrier frequencies  $f$  and electric field strengths  $E$  in the absence of any pressure-driven flow. Figure 11(a) shows an example of the oscillation cycle of a dead bacterium at  $f = 0.1$  Hz with  $E = 1,041$  V/m. Bacteria are observed for 30 s with a framerate of 30 fps, and the displacement is again tracked using ImageJ. Figure 11(b) shows the displacement amplitudes  $A_{EK}$  of a live and a dead bacterium collected at  $f = 0.1$  Hz for five different electric field strengths. The dashed lines show a linear fit passing through the origin. No significant changes in  $A_{EK}$  are found between live and dead bacteria, suggesting that neither

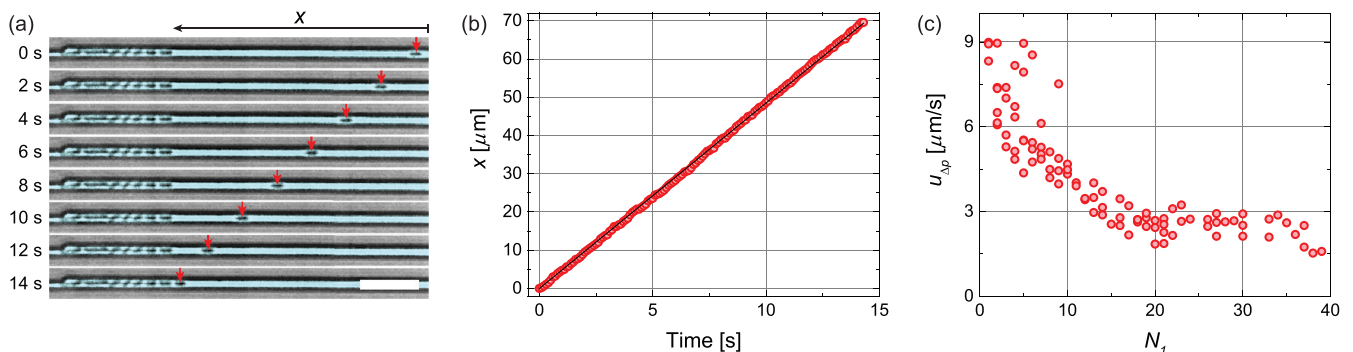


FIG. 10. (a) Time-lapse images of a bacterium in a microchannel in pressure-driven flow. The false colored image shows the broth medium in blue. The scale bar is  $10 \mu\text{m}$ . (b) A set of position vs. time data obtained from optical tracking (red symbols). The linear fit (black line) provides the velocity of the bacterium. (c) The flow velocity as a function of the number  $N_1$  of bacteria already trapped in a microchannel. Each data point is determined from a measurement on a single bacterium.

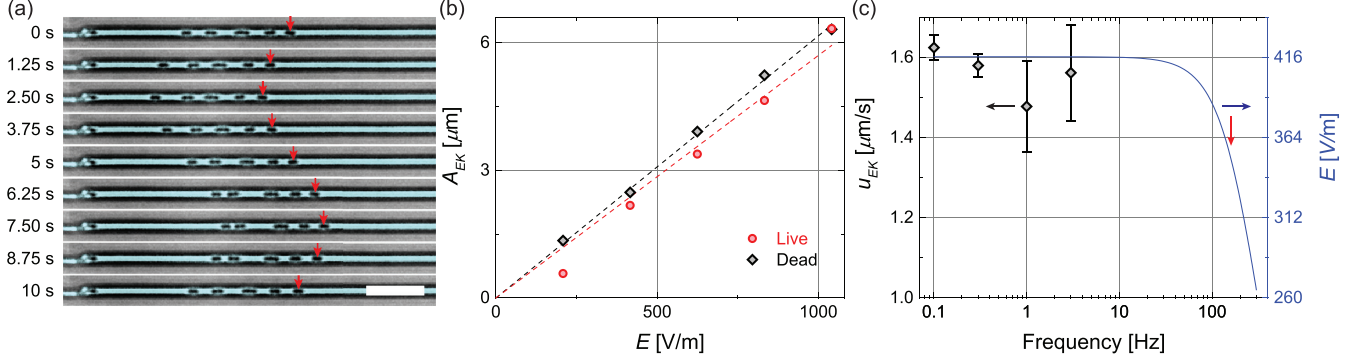


FIG. 11. (a) Time-lapse images of the electrokinetic movements of bacteria in a microchannel. Here the velocity  $u_{EK}$  is determined from optical tracking of these movements at  $f = 0.1$  Hz and  $E = 1,041$  V/m. The false colored image shows the broth medium in blue. The scale bar is  $10 \mu\text{m}$ . (b) Comparison showing that electrokinetic forces acting on live and dead bacteria are very close in magnitude. Here we measure the displacement amplitude  $A_{EK}$  of live and dead bacteria at different electric field strengths at a frequency of  $0.1$  Hz. (c) Electrokinetic velocity as a function of frequency. The black symbols show measurements taken at four different frequencies. The blue curve shows the frequency dependence of  $E(f)$ . The red arrow indicates that the largest electric field strength used in our experiments at  $f_o = 160$  Hz is  $E(f_o) = 350$  V/m.

electrokinetic forces nor friction coefficients are affected by fixation with glutaraldehyde.

Our goal is to determine the largest value of the electrokinetic velocity in our experiments obtained at an applied electric field strength of  $E(f_o) = 350$  V/m at the carrier frequency of  $f_o = 160$  Hz. Because of resolution limits, we cannot directly measure this quantity. Instead, we measure the displacement amplitudes of a single bacterium at low frequencies and high electric fields. The value of  $E(f_o)$  is slightly lower than  $E(f \lesssim 10 \text{ Hz})$  due to attenuation by the parasitic capacitance in our system, as shown by the calculated blue curve in Fig. 11(c). For  $f \leq 3$  Hz, we convert the displacement amplitudes to velocity via  $u_{EK}(f) = 2\pi f A_{EK}(f)$ . We find  $u_{EK}(f \leq 3 \text{ Hz}) \approx 1.6 \mu\text{m/s}$ , corresponding to an electrokinetic mobility of  $\mu_{EK} \approx 3.8 \times 10^{-9} \text{ m}^2/(\text{V s})$  through the relation  $u_{EK}(f) \approx \mu_{EK} E(f)$ . Using this mobility value, we find the maximum electrokinetic velocity at  $160$  Hz to be  $u_{EK}(f_o) \approx 1.3 \mu\text{m/s}$ .

In summary, the electrokinetic force acting on the bacteria is measured to be smaller than the drag force due to the pressure-driven flow. Hence, the bacteria are pushed toward the nanoconstrictions in the microchannels. Once loaded under the high-pressure flow, the cells tend to stay in place and not move at all.

### 3. Time constants

There are a number of time constants in the system, in addition to the charge relaxation time of a single bacterium. Here we discuss these and provide estimates for each. Since there is a steady flow of velocity  $2.5 \mu\text{m}$  from inlet to outlet, the microchannels get flushed in a timescale  $\tau_f \sim \frac{l}{u_{\Delta p}} \sim 40$  s. The diffusion time constant,  $\tau_d \sim \frac{l^2}{D} \sim 10$  s, where  $D \sim 10^{-9} \text{ m}^2/\text{s}$  is the diffusion coefficient for small inorganic cations in water [81]. The charge relaxation time of the bacteria and  $\tau_d$  are of the same order. Finally, ions drift in the microchannels due to the electric field. Since we are using an ac field, the cations drift on the average  $l_\mu \sim \frac{\mu E(f_o)}{2f_o} \sim 110$  nm during half of a cycle of the oscillating field. Here the mobility

for small cations is taken as  $\mu \sim 10^{-7} \text{ m}^2/(\text{V s})$  [82] and the largest electric field value is used for the estimate. Since  $l_\mu \ll l$ , drift does not play a role in our observations.

### 4. Temperature increase due to Joule heating

We estimate the temperature increase in our microchannels due to Joule heating using a control volume approach. We use one of the ten channels as the control volume. Conservation of energy per unit time in steady state leads to

$$\dot{m}c_p(T_\infty - T_C) + I_1^2 R_1 - q''A = 0. \quad (\text{D2})$$

Here  $\dot{m}$  is the mass flow rate,  $c_p$  is the specific heat capacity of the broth,  $T_\infty = 310$  K is the temperature of our sample far removed from the channel,  $T_C$  is the microchannel temperature,  $I_1 = \frac{I}{10} \approx 1.7$  nA is the maximum current passing through the channel,  $R_1 = 10R \approx 31 \text{ M}\Omega$  is the channel resistance,  $q''$  is the heat flux, and  $A$  is the relevant area of channel wall. The mass flow rate can be expressed as  $\dot{m} = \rho_l w h u_{\Delta p}$ , where  $\rho_l \approx 1000 \text{ kg/m}^3$  is the density of the broth. We use  $c_p \approx 4000 \text{ J}/(\text{kg K})$  [83]. We simplify the calculation of  $q''$  using a one-dimensional model by neglecting any heat flux through the PDMS due to the smaller thickness  $d = 1$  mm and higher thermal conductivity of the glass substrate [84]. The heat flux through the glass substrate can then be approximated as

$$q'' \approx k \left( \frac{T_C - T_\infty}{d} \right). \quad (\text{D3})$$

Here  $k = 1.4 \text{ W}/(\text{m K})$  is the thermal conductivity of glass. With the contact area between broth and glass substrate  $A = lw$ , the channel temperature can then be expressed as

$$T_C = T_\infty + \frac{I_1^2 R_1}{\dot{m}c_p + k \frac{lw}{d}}. \quad (\text{D4})$$

For the maximum current used in our experiments, the temperature in the microchannels increases by  $\sim 3.2 \times 10^{-4}$  K.

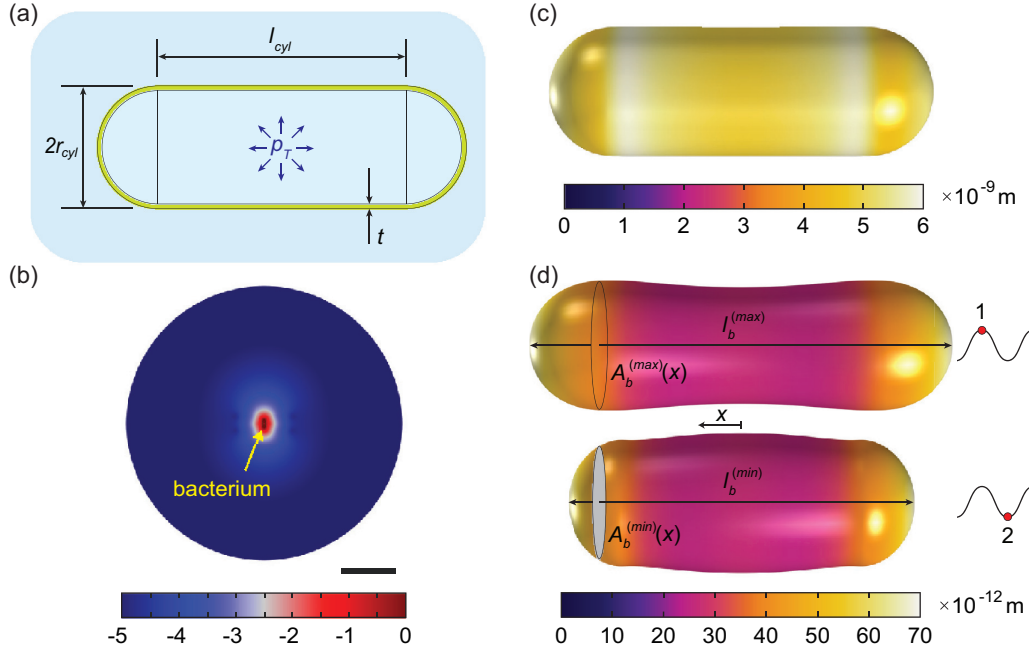


FIG. 12. (a) Cross section of a bacterium (*K. pneumoniae*) immersed in water. The bacterium is modeled as a hollow cylinder with wall thickness  $t$ , length  $l_{\text{cyl}}$ , and radius  $r_{\text{cyl}}$ , with a hollow semisphere of the same thickness on each end. The inside of the bacterium is modeled as water under turgor pressure  $p_T$  [34]. (b) In the model, the bacterium is immersed in a sphere of water with  $100 \mu\text{m}$  diameter to capture all viscous, acoustic and thermal losses. The logarithmic plot of the normalized fluid velocity shows that the fluid can be assumed as quiescent at the boundary of our model. The scale bar is  $20 \mu\text{m}$ . (c) Steady-state expansion due to turgor pressure. The induced tension in the cell wall affects the eigenmode oscillations. (d) Maximum (1) and minimum (2) deformations during the oscillation cycle of the eigenmode at  $8.26 \text{ MHz}$ . The amplitude field shown gives a strain energy that is equal to the thermal energy at  $310 \text{ K}$ . The respective lengths and cross sections of the bacterium are represented as  $l_b^{(\text{max})}$ ,  $l_b^{(\text{min})}$ ,  $A_b^{(\text{max})}$ , and  $A_b^{(\text{min})}$ . The eigenmode deformations are artificially scaled up by a scale factor of 2000 for enhancing the contrast.

## 5. Resistance fluctuations due to nanomechanical fluctuations of a bacterium

### a. Finite element model

A finite element model of the nanomechanical dynamics of a *K. pneumoniae* cell in water is created using COMSOL Multiphysics<sup>TM</sup>. The bacterium is modeled as a hollow cylinder with length  $l_{\text{cyl}} = 2 \mu\text{m}$ , radius  $r_{\text{cyl}} = 500 \text{ nm}$ , and wall thickness  $t = 26 \text{ nm}$ , with two hemispheres of the same radius and thickness attached to both ends, as shown in Fig. 12(a) [34]. The cell wall is modeled as a linear elastic material with Young's modulus  $E = 49 \text{ MPa}$ , Poisson's ratio  $\nu = 0.16$ , and density  $\rho_b = 1,100 \text{ kg/m}^3$  [34,85,86]. The inside of the bacterium is modeled as water under turgor pressure ( $p_T = 29 \text{ kPa}$ ) [34]. The bacterium is surrounded by a sphere of water under atmospheric pressure. Both bodies of water are modeled as viscous compressible Newtonian fluids, and the diameter of the surrounding water sphere is chosen as  $100 \mu\text{m}$  such that all viscous and thermal losses can be captured within the model [Fig. 12(b)] [87]. A prestressed eigenfrequency study is used, which consists of a stationary solver followed by an eigenfrequency solver. For the stationary step, a boundary load is placed on the inner wall of the bacterium to model the expansion due to the turgor pressure. For the eigenfrequency step, a multiphysics coupler connects the Solid Mechanics and Thermoviscous Acoustics modules.

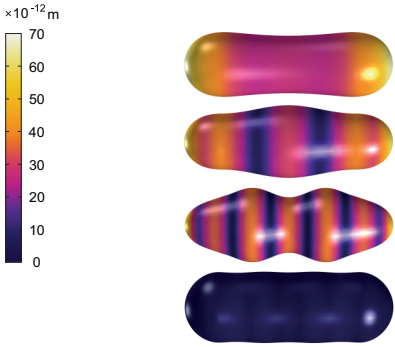

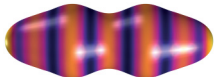

The matrix  $\mathbf{x}_0$  contains the initial radial and axial coordinates for each of the  $N$  finite elements comprising the

axisymmetric cell surface. The turgor pressure expands the shell coordinates to  $\mathbf{x}'_0$  [Fig. 12(c)]. The time-dependent coordinates of the  $N$  finite elements during eigenmode oscillations are of the form  $\mathbf{x}'_0 + \mathbf{a}_n \cos \omega_n t$ , where  $\mathbf{a}_n$  is the modal amplitude, i.e., the amplitude along the eigenvector, and  $\omega_n$  is the eigenfrequency. An example of the deformations in one of the eigenmodes is shown in Fig. 12(d).

In order to make more quantitative comparisons, we will use the strain energy  $U$ . Strain energy will allow us to express a given rms oscillation amplitude in units of the strain energy  $U^{(\text{th})}$  of the thermal fluctuations and define an approximate effective temperature. To this end, we can easily find the modal amplitude  $\mathbf{a}_n^{(\text{th})}$  for each mode, which results in a strain energy of  $U^{(\text{th})} = k_B T$ , where  $k_B$  is the Boltzmann constant and  $T = 310 \text{ K}$  is the equilibrium temperature. One could think of  $U^{(\text{th})}$  as the approximate energy of a fixed bacterium—assuming the physical properties of the fixed bacterium do not change upon chemical fixing.

In live bacteria, nanomechanical fluctuations originating from active processes must be dominant compared to the thermal fluctuations. Nanoscale movements due to active processes has been observed in different human and animal cells [58–63], giant vesicles [64], yeast [65], as well as motile and nonmotile bacteria [66,88]. For nonmotile bacteria, these active processes include, but are not limited to, the activity of ion pumps [89], the movement of proteins across the outer membrane [90,91], and the fluctuations in the cytoskeleton (e.g., due to motor proteins) [92]. A live

TABLE I. Estimated parameters for the simulated nanomechanical eigenmodes of *K. pneumoniae*. We only show selected eigenmodes which have the largest deformations. The first column shows the deformation of the bacterium in the eigenmode. The deformations are artificially scaled up by a scale factor of 2000 for better contrast. The second and third columns show the eigenfrequency and the quality factor of the mode, respectively. The fourth column lists the effective temperature for the strain energy, determined by equating the strain energy to  $k_B T_{\text{eff}}$ , as described in the text. The last column is the rms value of the resistance fluctuations  $r_{300}$  caused by 300 bacteria at a strain energy of  $k_B T_{\text{eff}}$ . The bottom row shows the experimental values for comparison.

Eigenmode	$f$ [MHz]	$Q$	$T_{\text{eff}}$ [K]	$r_{300}$ [ $\Omega$ ]
	8.26	3.09	310	0.766
	11.88	2.19	310	0.524
	15.95	2.15	310	0.219
	18.48	1.69	310	0.012
Experiment	—	—	$2.4 \times 10^7$	214.0

bacterium would thus have a strain energy  $U^{(\text{act})}$  that is significantly larger than the thermal strain energy  $U^{(\text{th})} = k_B T$ , discussed above. The corresponding effective temperature,  $k_B T_{\text{eff}} = U^{(\text{act})}$ , is also larger than the equilibrium temperature  $T = 310$  K.

### b. Conversion of deformations into resistance changes

The rms resistance change  $r$  across a single microchannel with cross-sectional area  $A_c = 4 \mu\text{m}^2$  and length  $l_c = 100 \mu\text{m}$  caused by one bacterium oscillating coherently with an energy equal to its equilibrium thermal energy can be approximated as

$$r \approx \frac{\rho}{2\sqrt{2}} \left| \int_{-l_b^{(\text{max})}/2}^{l_b^{(\text{max})}/2} \frac{dx}{A_c - A_b^{(\text{max})}(x)} - \int_{-l_b^{(\text{min})}/2}^{l_b^{(\text{min})}/2} \frac{dx}{A_c - A_b^{(\text{min})}(x)} - \frac{l_b^{(\text{max})} - l_b^{(\text{min})}}{A_c} \right|. \quad (\text{D5})$$

Here  $r$  is calculated by finding the difference in microchannel resistance between the maximum and minimum deformation states of the bacterium [shown as 1 and 2 in Fig. 12(d)]. The parameters  $l_b^{(\text{max})}$ ,  $l_b^{(\text{min})}$ ,  $A_b^{(\text{max})}$ , and  $A_b^{(\text{min})}$  can be understood as the respective bacterial lengths and cross sections of these deformed states. The value of  $\rho$  for LB broth has been determined as  $\rho \approx 1.2 \Omega\text{m}$  from previous measurements [25]. To account for the  $300 \pm 50$  bacteria in our experiments, we assume 30 bacteria in each of the ten microchannels, all oscillating in the same eigenmode. In this step, by assuming that the oscillations are not coherent but their noise powers are additive, we make a transition from eigenmode oscillations to fluctuations. We calculate the total rms resistance fluctuations in our system as  $r_{300} \approx \frac{\sqrt{30}}{10} r$ .

We show the obtained values for  $r_{300}$  for four different eigenmodes in Table I. Here the modal strain energies are set to the thermal energy  $U^{(\text{th})}$  as described above, and hence

the effective temperature is 310 K. In order to compare the simulated results with the resistance fluctuations observed in our measurements, we find the experimental rms resistance fluctuations by calculating the variance of the resistance fluctuations from the measured PSDs [see Fig. 3] in the frequency range  $0.05 \text{ Hz} \leq f \leq 1 \text{ Hz}$  and properly subtracting the background noise power. The experimentally-determined value is  $r_{300} \approx 214 \Omega$ . We then find the modal amplitude  $\mathbf{a}_n^{(\text{hot})}$  from numerical simulations, at which the simulated  $r_{300}$  matches the experimental value based on Eq. (D5) and  $r_{300} \approx \frac{\sqrt{30}}{10} r$ . We do this exercise for the eigenmode with the largest thermal  $r_{300}$  value, i.e., the eigenmode at 8.26 MHz with  $r_{300} \approx 0.766 \Omega$ . The effective temperature  $T_{\text{eff}}$  at which active fluctuations attain the experimentally measured  $r_{300}$  is determined by using the strain energy ratios as  $\frac{U^{(\text{act})}}{U^{(\text{th})}} = \frac{T_{\text{eff}}}{310}$ . As a result, we obtain that  $T_{\text{eff}} \sim 10^7 \text{ K}$  for the bacteria in the experiments.

### c. Discussion

Our eigenfrequency and quality factor values for the first mode generally agree with those in other simulations where bacteria are modeled as floating shells filled with and surrounded by water [93–95]; they are, however, significantly lower than the values obtained in simulations where bacteria are modeled as solid spheres attached to a substrate and surrounded by air [96]. We also note that the following factors seem to affect the results in the literature: (1) the material properties of the bacterial shell, (2) boundary conditions, and (3) computing algorithm. We are not sure which physical mechanisms dominate the energy dissipation. We also don't know whether or not the  $Q$  factors observed here and in the literature are reasonable.

Because of a lack of understanding of the nanomechanical fluctuations of bacteria at low frequencies, our model comes with shortcomings and provides only some level of comparison. First, we are essentially comparing thermal fluctuations



with  $1/f$  noise. Thermal fluctuations in this system are spread over a broad bandwidth on the order of a few MHz, as suggested by the  $Q$  values, whereas the observed  $1/f$  noise is at low frequency within 2 Hz from dc. Second, we assume that the active cell movements come with the spatial deformations of the eigenmodes—even though active processes should excite the cell deformations at random locations. Regardless, the enormous difference between the observed and computed strain energies has convinced us that nanomechanical motion is an unlikely source for our observations.

## APPENDIX E: ELECTRICAL NOISE CALCULATIONS

### 1. Determining charge noise from resistance noise

As noted in the main text, the relationship between the PSD of the resistance fluctuations,  $S_R(f)$ , and the PSD of the carrier number fluctuations,  $S_n(f)$ , is given by Eq. (11). As shown in Eq. (11), both  $S_R(f)$  and  $R_m$  are resultant values for the entire microfluidic resistor, i.e., the ten microchannels in parallel. It is easy to show that  $\frac{S_R(f)}{R_m^2} = \frac{S_R^{(1)}(f)}{R_1^2}$ , where  $R_1$  and  $S_R^{(1)}(f)$  are respectively the resistance value and the PSD of the resistance fluctuations of a single microchannel (out of the ten). Since  $R_1 = \rho \frac{l}{A_c} = \rho \frac{l}{wh}$ ,  $R_m = \rho \frac{l}{10A_c}$ ,  $S_R^{(1)}(f) = S_\rho \frac{l^2}{A_c^2}$ , and  $S_R(f) = S_\rho \frac{l^2}{100A_c^2}$ , we arrive at  $S(f) = \frac{S_R(f)}{R_m^2} = \frac{S_R^{(1)}(f)}{R_1^2} = \frac{S_\rho}{\rho^2}$  for spatially uniform fluctuations. Here  $S_\rho$  is the PSD of the resistivity fluctuations. We make estimates by focusing on a single microchannel (out of the ten), in which  $n \approx 4 \times 10^{10}$  at the 85 mM NaCl concentration of LB. There are  $N \approx 30$  bacteria in a single microchannel. The result holds if we focus on the entire microfluidic resistor, where  $n \approx 4 \times 10^{11}$  and  $N \approx 300$ .

### 2. Estimating voltage noise from charge noise

To find the value of  $\tau$ , we turn to previous work [14]. In Fig. 3 of [14], the authors have shown that spontaneous electrical blinks in bacteria decay exponentially on timescales  $10 \text{ s} \lesssim \tau \lesssim 30 \text{ s}$ . These timescales are obtained by fitting the autocorrelation function of the fluorescence intensity measured from single bacterial cells to a single exponential decay. For  $\tau = 10 \text{ s}$  and  $30 \text{ s}$ , we find the rms value of the fluctuations in the number of ions for one bacterium is  $\Delta n_{rms}^{(1)} \approx 1.3 \times 10^6$ , based on our data shown in Fig. 6.

In the second approach provided in the main text, we estimate the noise,  $e_n$ , in the membrane potential,  $V_{mem}$ , from the fluctuations in the intracellular ion concentrations. We assume that the ions are distributed uniformly inside and outside the cell. We focus on the  $\text{K}^+$ ,  $\text{Na}^+$ , and  $\text{Cl}^-$  because these three make the largest contribution to the steady-state value of  $V_{mem}$  (i.e., the resting membrane potential). The Goldman-Hodgkin-Katz (GHK) equation [12] provides the value of  $V_{mem}$  as

$$V_{mem} = \frac{RT}{F} \ln \left( \frac{p_K[\text{K}^+]_o + p_{\text{Na}}[\text{Na}^+]_o + p_{\text{Cl}}[\text{Cl}^-]_i}{p_K[\text{K}^+]_i + p_{\text{Na}}[\text{Na}^+]_i + p_{\text{Cl}}[\text{Cl}^-]_o} \right). \quad (\text{E1})$$

Here  $R = 8.314 \text{ J K}^{-1} \text{ mol}^{-1}$  is the universal gas constant,  $T \approx 310 \text{ K}$  is the temperature,  $F = 96,485 \text{ C mol}^{-1}$  is Faraday's constant;  $p_K$ ,  $p_{\text{Na}}$ , and  $p_{\text{Cl}}$  are, respectively, the relative membrane permeabilities;  $[\text{K}^+]_i$ ,  $[\text{Na}^+]_i$ , and  $[\text{Cl}^-]_i$  are, respectively, the intracellular ion concentrations; and  $[\text{K}^+]_o$ ,  $[\text{Na}^+]_o$ , and  $[\text{Cl}^-]_o$  are, respectively, the uniform extracellular ion concentrations for  $\text{K}^+$ ,  $\text{Na}^+$ , and  $\text{Cl}^-$ .

For a bacterium, the relative membrane permeabilities are  $p_K:p_{\text{Na}}:p_{\text{Cl}} = 1:0.05:0.45$ ; the intracellular ion concentrations are  $[\text{K}^+]_i = 150 \text{ mM}$ ,  $[\text{Na}^+]_i = 15 \text{ mM}$ , and  $[\text{Cl}^-]_i = 10 \text{ mM}$ ; the extracellular ion concentrations are  $[\text{K}^+]_o = 4 \text{ mM}$ ,  $[\text{Na}^+]_o = 145 \text{ mM}$ , and  $[\text{Cl}^-]_o = 110 \text{ mM}$ . By substituting the values of the relative permeabilities  $p_X$ , the intracellular ion concentrations  $[\text{X}]_i$ , and the extracellular ion concentrations  $[\text{X}]_o$  into Eq. (E1), we find the steady-state value of the membrane potential to be  $V_{mem} \approx -67.92 \text{ mV}$ . For a given ion X with charge  $z$ , we use  $E_X = \frac{RT}{zF} \ln \left( \frac{[\text{X}]_o}{[\text{X}]_i} \right)$  to find the equilibrium potentials (Nernst potentials). This yields  $-96.81 \text{ mV}$ ,  $60.60 \text{ mV}$ , and  $-64.05 \text{ mV}$  for  $\text{K}^+$ ,  $\text{Na}^+$ , and  $\text{Cl}^-$ , respectively.

To find the total rms change in  $V_{mem}$  due to fluctuations in the concentration of each ion, we calculate the change (fluctuation) in potential from Eq. (E1) with respect to each  $[\text{X}]_i$  as  $\frac{\partial V_{mem}}{\partial [\text{X}]_i} \Delta[\text{X}]_i$ , square each fluctuation value, add the squares, and then take the square root of the sum. Then, we find the total rms change  $e_n$  described by Eq. (12). As shown in Eq. (12),  $\Delta[\text{K}^+]_i$ ,  $\Delta[\text{Na}^+]_i$ , and  $\Delta[\text{Cl}^-]_i$  are the rms fluctuations in the intracellular ion concentrations; the other parameters are as listed above for Eq. (E1). For a bacterium with volume  $V_b \sim 10^{-18} \text{ m}^3$ , the rms fluctuations in intracellular ion concentration for each ion is estimated from our experiments to be of order  $\Delta[\text{K}^+]_i = \Delta[\text{Na}^+]_i = \Delta[\text{Cl}^-]_i \sim \frac{\Delta n_{rms}^{(1)}}{V_b} \sim 10^{24} \text{ m}^{-3}$ . The extracellular ion concentrations are assumed to remain unchanged. Then, by substituting all the values into Eq. (12), we find  $e_n \sim 1.3 \text{ mV}$ .

- [1] L. Galera-Laporta, C. J. Comerci, J. Garcia-Ojalvo, and G. M. Süel, Ionobiology: The functional dynamics of the intracellular metallo, with lessons from bacteria, *Cell Syst.* **12**, 497 (2021).
- [2] N. Korolev, How potassium came to be the dominant biological cation: Of metabolism, chemiosmosis, and cation selectivity since the beginnings of life, *BioEssays* **43**, 2000108 (2021).
- [3] G. N. Bruni, R. A. Weekley, B. J. Dodd, and J. M. Kralj, Voltage-gated calcium flux mediates *Escherichia coli*

mechanosensation, *Proc. Natl. Acad. Sci. USA* **114**, 9445 (2017).

- [4] A. Anishkin, S. H. Loukin, J. Teng, and C. Kung, Feeling the hidden mechanical forces in lipid bilayer is an original sense, *Proc. Natl. Acad. Sci. USA* **111**, 7898 (2014).
- [5] A. Prindle, J. Liu, M. Asally, J. Garcia-Ojalvo, and G. M. Süel, Ion channels enable electrical communication in bacterial communities, *Nature (London)* **527**, 59 (2015).

- [6] P. Mitchell, Coupling of phosphorylation to electron and hydrogen transfer by a chemi-osmotic type of mechanism, *Nature (London)* **191**, 144 (1961).
- [7] H. Strahl and L. W. Hamoen, Membrane potential is important for bacterial cell division, *Proc. Natl. Acad. Sci. USA* **107**, 12281 (2010).
- [8] D. L. Dong-yeon, L. Galera-Laporta, M. Bialecka-Fornal, E. C. Moon, Z. Shen, S. P. Briggs, J. Garcia-Ojalvo, and G. M. Süel, Magnesium flux modulates ribosomes to increase bacterial survival, *Cell* **177**, 352 (2019).
- [9] P. D. Damper and W. Epstein, Role of the membrane potential in bacterial resistance to aminoglycoside antibiotics, *Antimicrobial Agents Chemotherapy* **20**, 803 (1981).
- [10] D. C. Gadsby, Ion channels versus ion pumps: The principal difference, in principle, *Nat. Rev. Mol. Cell Biol.* **10**, 344 (2009).
- [11] C.-Y. Yang, M. Bialecka-Fornal, C. Weatherwax, J. W. Larkin, A. Prindle, J. Liu, J. Garcia-Ojalvo, and G. M. Süel, Encoding membrane-potential-based memory within a microbial community, *Cell Syst.* **10**, 417 (2020).
- [12] J. M. Benarroch and M. Asally, The microbiologist's guide to membrane potential dynamics, *Trends Microbiol.* **28**, 304 (2020).
- [13] Z. Schofield, G. N. Meloni, P. Tran, C. Zerfass, G. Sena, Y. Hayashi, M. Grant, S. A. Contera, S. D. Minter, M. Kim *et al.*, Bioelectrical understanding and engineering of cell biology, *J. R. Soc. Interface.* **17**, 20200013 (2020).
- [14] J. M. Kralj, D. R. Hochbaum, A. D. Douglass, and A. E. Cohen, Electrical spiking in *Escherichia coli* probed with a fluorescent voltage-indicating protein, *Science* **333**, 345 (2011).
- [15] M. Queralt-Martín, D. A. Perini, and A. Alcaraz, Specific adsorption of trivalent cations in biological nanopores determines conductance dynamics and reverses ionic selectivity, *Phys. Chem. Chem. Phys.* **23**, 1352 (2020).
- [16] L. J. DeFelice, *Introduction to Membrane Noise* (Springer, New York, 1981).
- [17] J. C. Weaver and R. D. Astumian, The response of living cells to very weak electric fields: The thermal noise limit, *Science* **247**, 459 (1990).
- [18] T. Xie, Y.-D. Chen, P. Marszalek, and T. Y. Tsong, Fluctuation-driven directional flow in biochemical cycle: Further study of electric activation of Na, K pumps, *Biophys. J.* **72**, 2496 (1997).
- [19] L. Endresen, K. Hall, J. Høyve, and J. Myrheim, A theory for the membrane potential of living cells, *Eur. Biophys. J.* **29**, 90 (2000).
- [20] T. J. Hund, J. P. Kucera, N. F. Otani, and Y. Rudy, Ionic charge conservation and long-term steady state in the Luo-Rudy dynamic cell model, *Biophys. J.* **81**, 3324 (2001).
- [21] L. Shabala, T. Ross, I. Newman, T. McMeekin, and S. Shabala, Measurements of net fluxes and extracellular changes of H<sup>+</sup>, Ca<sup>2+</sup>, K<sup>+</sup>, and NH<sub>4</sub><sup>+</sup> in *Escherichia coli* using ion-selective microelectrodes, *J. Microbiol. Methods* **46**, 119 (2001).
- [22] L. Shabala, J. Bowman, J. Brown, T. Ross, T. McMeekin, and S. Shabala, Ion transport and osmotic adjustment in *Escherichia coli* in response to ionic and non-ionic osmotica, *Environ. Microbiol.* **11**, 137 (2009).
- [23] S. M. Bezrukov and M. Winterhalter, Examining Noise Sources at the Single-Molecule Level: 1/f Noise of an Open Maltoporin Channel, *Phys. Rev. Lett.* **85**, 202 (2000).
- [24] J. H. Scofield, a method for measuring low-frequency resistance fluctuation spectra, *Rev. Sci. Instrum.* **58**, 985 (1987).
- [25] Y. Yang, K. Gupta, and K. L. Ekinci, All-electrical monitoring of bacterial antibiotic susceptibility in a microfluidic device, *Proc. Natl. Acad. Sci. USA* **117**, 10639 (2020).
- [26] R. F. Voss and J. Clarke, Flicker (1/f) noise: Equilibrium temperature and resistance fluctuations, *Phys. Rev. B* **13**, 556 (1976).
- [27] P. Dutta and P. Horn, Low-frequency fluctuations in solids: 1/f noise, *Rev. Mod. Phys.* **53**, 497 (1981).
- [28] P. A. W. E. Verleg and J. I. Dijkhuis, Resistance fluctuations in hydrogenated amorphous silicon: Thermal equilibrium, *Phys. Rev. B* **58**, 3904 (1998).
- [29] C. Tasserit, A. Koutsioubas, D. Lairez, G. Zalczer, and M.-C. Clochard, Pink Noise of Ionic Conductance through Single Artificial Nanopores Revisited, *Phys. Rev. Lett.* **105**, 260602 (2010).
- [30] C. Wen, S. Zeng, K. Arstila, T. Sajavaara, Y. Zhu, Z. Zhang, and S.-L. Zhang, Generalized noise study of solid-state nanopores at low frequencies, *ACS Sensors* **2**, 300 (2017).
- [31] P. R. Rocha, P. Schlett, U. Kintzel, V. Mailänder, L. K. Vandamme, G. Zeck, H. L. Gomes, F. Biscarini, and D. M. De Leeuw, Electrochemical noise and impedance of Au electrode/electrolyte interfaces enabling extracellular detection of glioma cell populations, *Sci. Rep.* **6**, 34843 (2016).
- [32] M. Tsutsui, S. Rahong, Y. Iizumi, T. Okazaki, M. Taniguchi, and T. Kawai, Single-molecule sensing electrode embedded in-plane nanopore, *Sci. Rep.* **1**, 46 (2011).
- [33] T. Maleki, S. Mohammadi, and B. Ziaie, A nanofluidic channel with embedded transverse nanoelectrodes, *Nanotechnology* **20**, 105302 (2009).
- [34] H. Zhang, H. Wang, J. J. Wilksch, R. A. Strugnell, M. L. Gee, and X.-Q. Feng, Measurement of the interconnected turgor pressure and envelope elasticity of live bacterial cells, *Soft Matter* **17**, 2042 (2021).
- [35] J. M. Monteiro, P. B. Fernandes, F. Vaz, A. R. Pereira, A. C. Tavares, M. T. Ferreira, P. M. Pereira, H. Veiga, E. Kuru, M. S. VanNieuwenhze *et al.*, Cell shape dynamics during the staphylococcal cell cycle, *Nat. Commun.* **6**, 8055 (2015).
- [36] G. McDonnell and A. D. Russell, Antiseptics and disinfectants: Activity, action, and resistance, *Clin. Microbiol. Rev.* **12**, 147 (1999).
- [37] J. H. Scofield, J. V. Mantese, and W. W. Webb, 1/f noise of metals: A case for extrinsic origin, *Phys. Rev. B* **32**, 736 (1985).
- [38] K. R. Foster and H. C. Lukaski, Whole-body impedance—What does it measure?, *Amer. J. Clin. Nutrition* **64**, 388S (1996).
- [39] R. Mancini, *Op Amps for Everyone: Design Reference* (Newnes, London, 2003).
- [40] R. M. Smeets, U. F. Keyser, N. H. Dekker, and C. Dekker, Noise in solid-state nanopores, *Proc. Natl. Acad. Sci. USA* **105**, 417 (2008).
- [41] S. Heerema, G. Schneider, M. Rozemuller, L. Vicarelli, H. Zandbergen, and C. Dekker, 1/f noise in graphene nanopores, *Nanotechnology* **26**, 074001 (2015).
- [42] Z. Siwy and A. Fuliński, Origin of 1/f<sup>α</sup> Noise in Membrane Channel Currents, *Phys. Rev. Lett.* **89**, 158101 (2002).
- [43] D. Fleetwood, 1/f noise and defects in microelectronic materials and devices, *IEEE Trans. Nucl. Sci.* **62**, 1462 (2015).

- [44] A. N. Pal and A. Ghosh, Resistance Noise in Electrically Biased Bilayer Graphene, *Phys. Rev. Lett.* **102**, 126805 (2009).
- [45] D. P. Hoogerheide, S. Garaj, and J. A. Golovchenko, Probing Surface Charge Fluctuations with Solid-State Nanopores, *Phys. Rev. Lett.* **102**, 256804 (2009).
- [46] F. N. Hooge,  $1/f$  noise sources, *IEEE Trans. Electron Devices* **41**, 1926 (1994).
- [47] F. N. Hooge,  $1/f$  noise is no surface effect, *Phys. Lett. A* **29**, 139 (1969).
- [48] J. Binette, M. Garon, P. Savard, M. McKee, and M. Buschmann, Tetrapolar measurement of electrical conductivity and thickness of articular cartilage, *J. Biomech. Eng.* **126**, 475 (2004).
- [49] J. L. Prieto, H.-W. Su, H. W. Hou, M. P. Vera, B. D. Levy, R. M. Baron, J. Han, and J. Voldman, Monitoring sepsis using electrical cell profiling, *Lab Chip* **16**, 4333 (2016).
- [50] H. Li, C. Multari, C. Palego, X. Ma, X. Du, Y. Ning, J. Buceta, J. C. Hwang, and X. Cheng, Differentiation of live and heat-killed *E. coli* by microwave impedance spectroscopy, *Sensors Actuators B* **255**, 1614 (2018).
- [51] See Supplemental Material at <http://link.aps.org/supplemental/10.1103/PhysRevE.105.064413> for additional data plots from supplemental measurements..
- [52] A. Hassibi, R. Navid, R. W. Dutton, and T. H. Lee, Comprehensive study of noise processes in electrode electrolyte interfaces, *J. Appl. Phys.* **96**, 1074 (2004).
- [53] V. Kara, C. Duan, K. Gupta, S. Kurosawa, D. J. Stearns-Kurosawa, and K. L. Ekinici, Microfluidic detection of movements of *Escherichia coli* for rapid antibiotic susceptibility testing, *Lab Chip* **18**, 743 (2018).
- [54] C. Lissandrello, L. Li, K. Ekinici, and V. Yakhot, Noisy transitional flows in imperfect channels, *J. Fluid Mech.* **778**, R3 (2015).
- [55] T. Y. Tsong, Electrical modulation of membrane proteins: Enforced conformational oscillations and biological energy and signal transductions, *Annu. Rev. Biophys. Biophys. Chem.* **19**, 83 (1990).
- [56] T.-D. Xie and T. Y. Tsong, Study of mechanisms of electric field-induced dna transfection. II. Transfection by low-amplitude, low-frequency alternating electric fields, *Biophys. J.* **58**, 897 (1990).
- [57] J. P. Stratford, C. L. Edwards, M. J. Ghanshyam, D. Malyshev, M. A. Delise, Y. Hayashi, and M. Asally, Electrically induced bacterial membrane-potential dynamics correspond to cellular proliferation capacity, *Proc. Natl. Acad. Sci. USA* **116**, 9552 (2019).
- [58] E. Ben-Isaac, Y. K. Park, G. Popescu, F. L. H. Brown, N. S. Gov, and Y. Shokef, Effective Temperature of Red-Blood-Cell Membrane Fluctuations, *Phys. Rev. Lett.* **106**, 238103 (2011).
- [59] H. Turlier, D. A. Fedosov, B. Audoly, T. Auth, N. S. Gov, C. Sykes, J.-F. Joanny, G. Gompper, and T. Betz, Equilibrium physics breakdown reveals the active nature of red blood cell flickering, *Nat. Phys.* **12**, 513 (2016).
- [60] A. Biswas, A. Alex, and B. Sinha, Mapping cell membrane fluctuations reveals their active regulation and transient heterogeneities, *Biophys. J.* **113**, 1768 (2017).
- [61] S. L. Nelson, D. T. Proctor, A. Ghasemloonia, S. Lama, K. Zareinia, Y. Ahn, M. R. Al-Saiedy, F. H. Green, M. W. Amrein, and G. R. Sutherland, Vibrational profiling of brain tumors and cells, *Theranostics* **7**, 2417 (2017).
- [62] S. Wu, X. Liu, X. Zhou, X. M. Liang, D. Gao, H. Liu, G. Zhao, Q. Zhang, and X. Wu, Quantification of cell viability and rapid screening anti-cancer drug utilizing nanomechanical fluctuation, *Biosens. Bioelectron.* **77**, 164 (2016).
- [63] V. R. Singh, Y. A. Yang, H. Yu, R. D. Kamm, Z. Yaqoob, and P. T. So, Studying nucleic envelope and plasma membrane mechanics of eukaryotic cells using confocal reflectance interferometric microscopy, *Nat. Commun.* **10**, 3652 (2019).
- [64] J.-B. Manneville, P. Bassereau, S. Ramaswamy, and J. Prost, Active membrane fluctuations studied by micropipet aspiration, *Phys. Rev. E* **64**, 021908 (2001).
- [65] R. G. Willaert, P. Vanden Boer, A. Malovichko, M. Alioschaper, K. Radotić, D. Bartolić, A. Kalauzi, M. I. Villalba, D. Sanglard, G. Dietler *et al.*, Single yeast cell nanomotions correlate with cellular activity, *Sci. Adv.* **6**, eaba3139 (2020).
- [66] G. Longo, L. Alonso-Sarduy, L. M. Rio, A. Bizzini, A. Trampuz, J. Notz, G. Dietler, and S. Kasas, Rapid detection of bacterial resistance to antibiotics using AFM cantilevers as nanomechanical sensors, *Nat. Nanotechnol.* **8**, 522 (2013).
- [67] C. Lissandrello, F. Inci, M. Francom, M. Paul, U. Demirci, and K. Ekinici, Nanomechanical motion of *Escherichia coli* adhered to a surface, *Appl. Phys. Lett.* **105**, 113701 (2014).
- [68] A. Van der Ziel, *Noise in Measurements* (Wiley, New York, 1976).
- [69] V. Mitin, L. Reggiani, and L. Varani, Generation-recombination noise in semiconductors, in *Noise Fluctuations Control Electron. Devices*, edited by A. A. Balandin (American Scientific Publishers, Los Angeles, 2002), 11–29.
- [70] S. R. McGuffee and A. H. Elcock, Diffusion, crowding & protein stability in a dynamic molecular model of the bacterial cytoplasm, *PLoS Comput. Biol.* **6**, e1000694 (2010).
- [71] M. Guragain, D. L. Lenaburg, F. S. Moore, I. Reutlinger, and M. A. Patrauchan, Calcium homeostasis in *Pseudomonas aeruginosa* requires multiple transporters and modulates swarming motility, *Cell Calcium* **54**, 350 (2013).
- [72] J. Liu, R. Martinez-Corral, A. Prindle, D.-Y. D. Lee, J. Larkin, M. Gabalda-Sagarra, J. Garcia-Ojalvo, and G. M. Süel, Coupling between distant biofilms and emergence of nutrient time-sharing, *Science* **356**, 638 (2017).
- [73] Y. Chao and T. Zhang, Optimization of fixation methods for observation of bacterial cell morphology and surface ultrastructures by atomic force microscopy, *Appl. Microbiol. Biotech.* **92**, 381 (2011).
- [74] A. D. Meade, C. Clarke, F. Draux, G. D. Sockalingum, M. Manfait, F. M. Lyng, and H. J. Byrne, Studies of chemical fixation effects in human cell lines using raman microspectroscopy, *Anal. Bioanal. Chem.* **396**, 1781 (2010).
- [75] P. Dmitruk, P. D. Mininni, A. Pouquet, S. Servidio, and W. H. Matthaeus, Emergence of very long time fluctuations and  $1/f$  noise in ideal flows, *Phys. Rev. E* **83**, 066318 (2011).
- [76] P. Marszalek, D. Liu, and T. Y. Tsong, Schwan equation and transmembrane potential induced by alternating electric field, *Biophys. J.* **58**, 1053 (1990).
- [77] K. Maswiwat, D. Wachner, R. Warnke, and J. Gimsa, Simplified equations for the transmembrane potential induced in ellipsoidal cells of rotational symmetry, *J. Phys. D* **40**, 914 (2007).
- [78] A. Sale and W. Hamilton, Effects of high electric fields on microorganisms: I. Killing of bacteria and yeasts, *Biochim. Biophys. Acta-General Subjects* **148**, 781 (1967).

- [79] B. Brambach, A. Michels, J. Franzke, and R. Kettler, Current density and conductivity dependent electroporation of *Escherichia coli* c600, *Prog. Biophys. Mol. Biol.* **111**, 46 (2013).
- [80] W. S. Rasband, ImageJ, U.S. National Institutes of Health, Bethesda, Maryland, <http://imagej.nih.gov/ij/> (2011).
- [81] E. Samson, J. Marchand, and K. A. Snyder, Calculation of ionic diffusion coefficients on the basis of migration test results, *Materials Struct.* **36**, 156 (2003).
- [82] B. J. Kirby, *Micro- and Nanoscale Fluid Mechanics: Transport in Microfluidic Devices* (Cambridge University Press, Cambridge, 2010).
- [83] B. Han and J. C. Bischof, Thermodynamic nonequilibrium phase change behavior and thermal properties of biological solutions for cryobiology applications, *J. Biomech. Eng.* **126**, 196 (2004).
- [84] D. Erickson, D. Sinton, and D. Li, Joule heating and heat transfer in poly (dimethylsiloxane) microfluidic systems, *Lab Chip* **3**, 141 (2003).
- [85] M. Mirzaali, I. Van Dongen, N. Tümer, H. Weinans, S. A. Yavari, and A. Zadpoor, *In-silico* quest for bactericidal but non-cytotoxic nanopatterns, *Nanotechnology* **29**, 43LT02 (2018).
- [86] P. Gerhardt and J. A. Judge, Porosity of isolated cell walls of *Saccharomyces cerevisiae* and *Bacillus megaterium*, *J. Bacteriol.* **87**, 945 (1964).
- [87] A. T. Liem, A. B. Ari, C. Ti, M. J. Cops, J. G. McDaniel, and K. L. Ekinci, Nanoflows induced by MEMS and NEMS: Limits of two-dimensional models, *Phys. Rev. Fluids* **6**, 024201 (2021).
- [88] I. Roslon, A. Japaridze, P. Steeneken, C. Dekker, and F. Alijani, Probing nanomotion of single bacteria with graphene drums, *Nat. Nanotechnol.* **17**, 637 (2022).
- [89] P. Dimroth, C. von Ballmoos, and T. Meier, Catalytic and mechanical cycles in F-ATP synthases, *EMBO Rep.* **7**, 276 (2006).
- [90] T. Lenn, M. C. Leake, and C. W. Mullineaux, Clustering and dynamics of cytochrome *bd*-I complexes in the *Escherichia coli* plasma membrane *in vivo*, *Mol. Microbiol.* **70**, 1397 (2008).
- [91] J. Spector, S. Zakharov, Y. Lill, O. Sharma, W. A. Cramer, and K. Ritchie, Mobility of BtuB and OmpF in the *Escherichia coli* outer membrane: Implications for dynamic formation of a translocon complex, *Biophys. J.* **99**, 3880 (2010).
- [92] R. G. Winkler and G. Gompper, The physics of active polymers and filaments, *J. Chem. Phys.* **153**, 040901 (2020).
- [93] P. V. Zinin and J. S. Allen III, Deformation of biological cells in the acoustic field of an oscillating bubble, *Phys. Rev. E* **79**, 021910 (2009).
- [94] Y. Choi, W.-S. Ohm, and Y.-T. Kim, Comment on deformation of biological cells in the acoustic field of an oscillating bubble, *Phys. Rev. E* **82**, 013901 (2010).
- [95] G. Tamadapu, A. Nordmark, and A. Eriksson, Resonances of a submerged fluid-filled spherically isotropic microsphere with partial-slip interface condition, *J. Appl. Phys.* **118**, 044903 (2015).
- [96] E. Gil-Santos, J. J. Ruz, O. Malvar, I. Favero, A. Lemaître, P. M. Kosaka, S. García-López, M. Calleja, and J. Tamayo, Optomechanical detection of vibration modes of a single bacterium, *Nat. Nanotechnol.* **15**, 469 (2020).